Published online 19 March 2013 Nucleic Acids Research, 2013, Vol. 41, No. 9 4765–4782
doi:10.1093/nar/gkt168

MBNL1 and PTB cooperate to repress splicing of Tpm1 exon 3

Clare Gooding[1], Christopher Edge[1], Mike Lorenz[2], Miguel B. Coelho[1], Mikael Winters[3], Clemens F. Kaminski[3], Dmitry Cherny[4], Ian C. Eperon[4] and Christopher W.J. Smith[1,*]

[1]Department of Biochemistry, University of Cambridge, CB2 1QW, UK, [2]Max Planck Institute of Molecular Cell Biology and Genetics, Pfotenhauerstr. 108, 01307 Dresden, Germany, [3]Department of Chemical Engineering and Biotechnology, University of Cambridge, CB2 3RA, UK and [4]Department of Biochemistry, University of Leicester, LE1 9HN, UK

Received January 17, 2013; Revised February 21, 2013; Accepted February 22, 2013

ABSTRACT

Exon 3 of the rat α-tropomyosin (*Tpm1*) gene is repressed in smooth muscle cells, allowing inclusion of the mutually exclusive partner exon 2. Two key types of elements affect repression of exon 3 splicing: binding sites for polypyrimidine tract-binding protein (PTB) and additional negative regulatory elements consisting of clusters of UGC or CUG motifs. Here, we show that the UGC clusters are bound by muscleblind-like proteins (MBNL), which act as repressors of *Tpm1* exon 3. We show that the N-terminal region of MBNL1, containing its four CCCH zinc-finger domains, is sufficient to mediate repression. The same region of MBNL1 can make a direct protein-to-protein interaction with PTB, and RNA binding by MBNL promotes this interaction, apparently by inducing a conformational change in MBNL. Moreover, single molecule analysis showed that MBNL-binding sites increase the binding of PTB to its own sites. Our data suggest that the smooth muscle splicing of *Tpm1* is mediated by allosteric assembly of an RNA–protein complex minimally comprising PTB, MBNL and their cognate RNA-binding sites.

INTRODUCTION

Alternative splicing is a key source of proteomic variation between different cell types, and it affects >90% of human genes (1,2). Many alternative splicing events have well-documented functional consequences and are tightly controlled with tissue and/or developmental specificity (3). Targeted investigations of individual model systems of regulated alternative splicing have provided detailed insights into molecular mechanisms of splicing regulation. These insights have been complemented by global approaches for profiling co-regulated splicing programs and pre-mRNA targets of individual RNA-binding proteins that regulate splicing (4–6). The mechanisms of tissue-specific alternative splicing have been particularly well investigated in mammalian neurons (7) and striated muscles (8).

Mutually exclusive exons 2 and 3 of the rat α-tropomyosin (*Tpm1*) gene have been used as a model system to investigate mechanisms of smooth muscle-regulated alternative splicing [Figure 1A; reviewed in (9)]. Exon 2 is selected in smooth muscle tissues, such as the vasculature, whereas exon 3 is exclusively selected in skeletal muscle, heart and brain (10,11). This event was singled out as an exemplar 'switch-event' in one of the first RNA-Seq–based global analyses of tissue-specific alternative splicing because of the magnitude of variation in the splicing pattern between tissues (1). In most tissue culture cells, transcripts with exon 3 are the default products (12), but in the smooth muscle, PAC1 cell line exon 2 is included (13,14). Default selection of exon 3 is driven by its strong branch point and pyrimidine tract elements (12) (denoted BP and P3 in Figure 1A). The exon 3 branch point is sufficiently close to exon 2 to prevent the two exons from being spliced together, thereby enforcing mutually exclusive behaviour (15). The switch to exon 2 selection involves regulated inhibition of exon 3 (11,14). Silencer elements consisting of two types of sequence motif are located in both introns flanking exon 3 (11,14,16,17). The branch point-associated P3 pyrimidine tract and a second downstream pyrimidine tract (denoted DY) bind the splicing regulator polypyrimidine tract-binding protein (PTB) (Figure 1A) (17–20). Two clusters of UGC motifs also lie adjacent to these pyrimidine tracts closer to the exon and are denoted here as 'D' and 'U' (previously referred to as Dugc and URE, respectively) (14,16).

The protein factor(s) that bind the UGC elements have been elusive. A 55 kDa protein that cross-linked to the U and D elements was observed in extracts from cells that

*To whom correspondence should be addressed. Tel: +44 1223 333655/65; Fax: +44 1223 766002; Email: cwjs1@cam.ac.uk

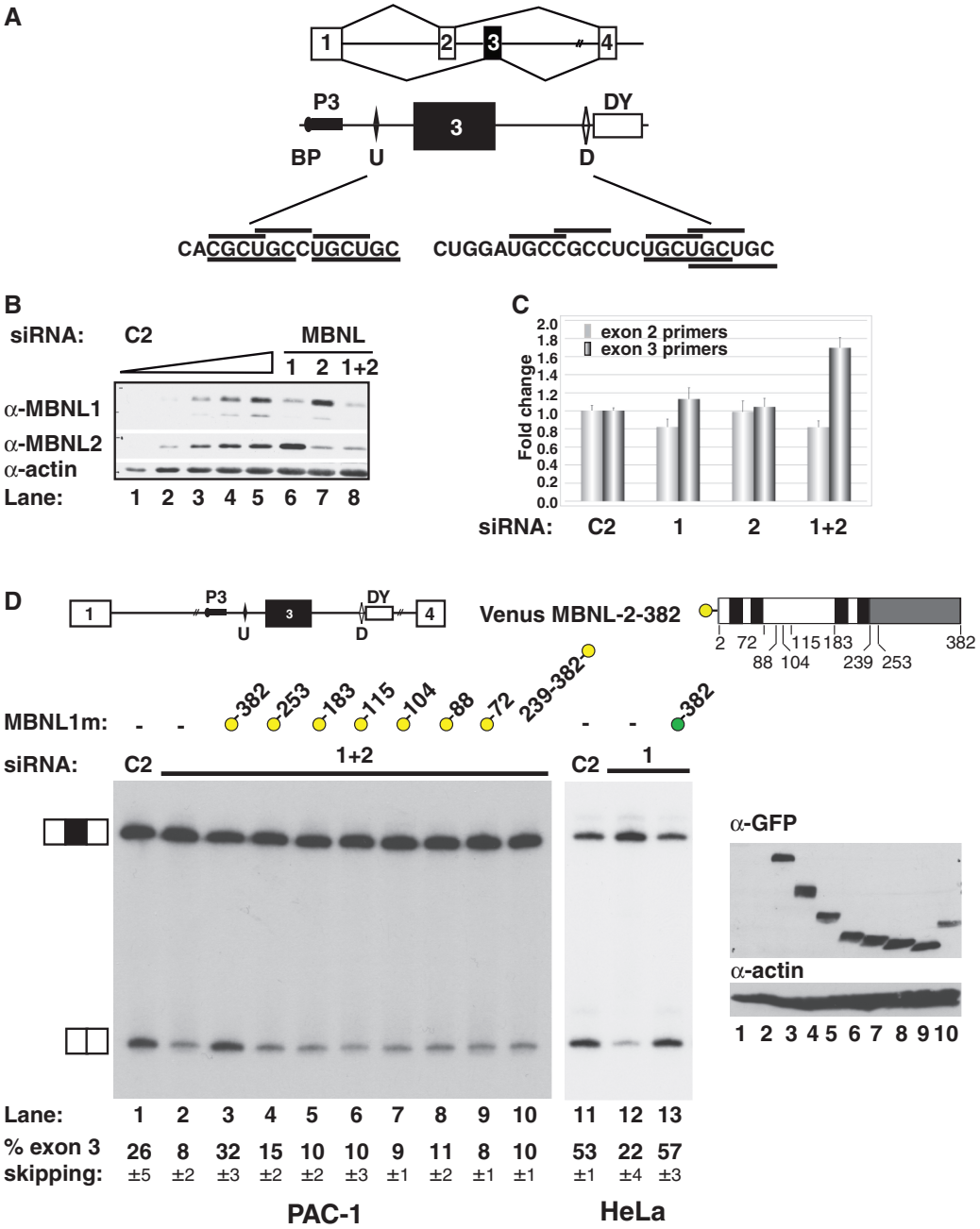

Figure 1. MBNL-like proteins repress *Tpm1* exon 3. (**A**) Schematic representation of the mutually exclusive splicing of *Tpm1* exons 2 and 3. The essential negative regulatory elements flanking exon 3 are indicated. The P3 and DY elements bind PTB and are denoted by black and white rectangles, respectively. The U and D elements are indicated by black and white diamonds, respectively, and their sequences are indicated. Matches to MBNL1 consensus sequences are underlined (YGCU(U/G)Y) and overlined (YGCY). (**B**) Western blot of siRNA knockdown, probed with α-MBNL1, α-MBNL2 or α-actin antibodies with a titration of control (C2) knockdown sample at 20, 40, 60, 80 and 100% (lanes 1–5) compared with knockdown of MBNL1, MBNL2 or MBNL1 plus MBNL2 (lanes 6–8). (**C**) qRT–PCR analysis of endogenous *Tpm1* on knockdown of MBNL1 and MBNL2. The histogram shows the fold change of exon 2 or exon 3 products comparing control siRNA (C2) with knockdown of MBNL1 (1), MBNL2 (2) or MBNL1 plus MBNL2 (1 + 2). (**D**) Schematic representation of *Tpm1* minigene reporter containing exons 1, 3 and 4 on the left, and Venus-tagged MBNL1 on the right. RT–PCR analysis of RNA isolated from PAC-1 cells (left panel) or HeLa cells (right panel) transfected with the *Tpm1* minigene reporter (lanes 1 and 11). In HeLa cells, the *Tpm1* mingene has a branch point mutation changing the wild-type sequence from GGCUAAC to GGCUGGC. Lanes 2–10, siRNA knockdown of MBNL1 and MBNL2 in PAC-1 cells together with overexpressed Venus–MBNL1 with the siRNA site mutated (lane 3), or various C-terminal truncations of Venus–MBNL1 (lanes 4–9); the yellow dots indicate Venus and the adjacent number represents the position of the C-terminal deletion. Lane 10 is transfected with an N-terminal MBNL1 deletion containing amino acids 239–382. Lanes 12 and 13, siRNA knockdown of MBNL1 in HeLa cells together with overexpressed GFP–MBNL1 with the siRNA site mutated, MBNL1m (lane 13). Right panel: anti-GFP (detects Venus) western blot; lane numbers correspond to those in the left panel.

had been selected for the ability to skip exon 3 (21), but the protein was not identified. The shuttling heterogeneous nuclear ribonucleoprotein (hnRNP)-like protein Raver1 (22) interacts with PTB, promotes skipping of exon 3 (23–25) and its first RNA Recognition Motif (RRM) domain can interact with an RNA containing both UGC and CUG motifs (26). However, the Raver1 RRM domains are not essential for its splicing repressor activity (23,24), and Raver1 knockout mice show unimpaired regulation of *Tpm1* splicing (27). The UGC elements resemble known binding sites for CUG-BP and ETR3 like factor (CELF) family proteins, such as CUG-BP (28). However, overexpression of CELF proteins promoted inclusion of exon 3 rather than skipping (16).

Muscleblind-like (MBNL) proteins have come to prominence as direct RNA-binding regulators of alternative splicing during development of striated muscles, in many cases antagonizing the activity of CELF proteins (29–34). MBNL proteins are characterized by four RNA-binding CCCH-type zinc-finger (ZF) domains at the N-terminal end, with ZF1 and 2, and ZF3 and 4 forming stable back-to-back di-domains (35,36). MBNL proteins were first characterized by their binding to CUG triplet repeat expansions that occur in the *DMPK* gene in myotonic dystrophy (37), and they were subsequently found to activate or repress splicing events that are misregulated in myotonic dystrophy (29–31,38,39). An MBNL-binding element YGCU(U/G)Y was initially identified in cardiac troponin T (*cTNT*) (30). Doped-SELEX based on known binding sites revealed a consensus YGCY, with a preference for UGCU (40), a sequence that occurs in multiple overlapping copies in CUG expansions. High-affinity binding requires at least two YGCY motifs with variable spacing (36,41). Structural analysis of MBNL1 ZF3 and 4 bound to 5′-CGCUGU-3′ RNA revealed that the GC step in particular is specifically recognized by both ZFs (36). MBNL proteins have not been implicated in smooth muscle-specific splicing events. However, the *Tpm1* U and D elements contain 3 and 4 YGCY motifs, respectively (overlined in Figure 1A).

Here, we show that MBNL proteins are necessary for regulated *Tpm1* exon 3 skipping. MBNL1 binds to both flanking UGC elements, and artificially tethered MBNL1 can restore the loss of function of either U or D element. Strikingly, we find that RNA binding by MBNL1 promotes its interaction with PTB, most likely by an RNA-induced conformational change. Regulated skipping of *Tpm1* exon 3, therefore, involves a network of interactions between PTB and MBNL proteins and the cognate silencer elements to which they bind on each side of the exon.

MATERIALS AND METHODS

Constructs

The minigene reporters, pTΔBP, with the branch point mutation, wild-type and the mutants in *cis*-regulatory elements have been described previously (16,42).

DNA constructs for UV cross-linking of the *Tpm1* regulatory elements were cloned into pGEM4Z for transcription with either T7 or SP6.

pEGFP–MBNL1 (amino acid 1–382; splice isoform a; NCBI accession number NP_066368) was provided by Tom Cooper (30). The THH2 siRNA target site of MBNL1 was mutated to CACGGAGTGTAAGTTTGC C. For expression and purification of recombinant MBNL1 in 293T cells, the coding sequence was cloned between XbaI and BamHI in pCGTHCF$_{FL}$T7 (43). For overexpression in HeLa and PAC-1 cells, the coding sequence for MBNL1 full length, amino acids 2–382, N-terminal amino acids 2–253, 2–183, 2–115, 2–102, 2–91, 2–72 and the C-terminal amino acids 239–382, was cloned using AvrII and MluI into pCIMS2–NLS–FLAG (23,44) with the MS2 coat protein for artificial tethering and without the MS2 coat protein for Glutatione S Transferase (GST) pull-down. For Förster resonance energy transfer (FRET) experiments and formaldehyde cross-linked lysates, full-length MBNL1 was cloned into the C1 version of Venus (Clontech) using Asp718 and BamHI and amino acids 2–182, 2–115, 2–104, 2–88 and 2–72 using EcoRI and SalI with the addition of a nuclear localization signal (NLS). Full-length MBNL1 and amino acids 239–382 were cloned into the N1 version using XhoI and Asp718 with the addition of an NLS. All PTB4 clones, full length, 12L and 34, were inserted into pmCherry-C1 using EcoRI and Asp718. The amino acids defining the different RRMs were taken from a previous study (45). C-terminal truncations of MBNL1 for expression of recombinant protein were cloned into pGEX4T using BamHI and EcoRI for amino acids 1–253 and EcoRI and SalI for amino acids 2–116, 2–91 and 2–72. Mutations of ZF1 and 2 in construct 2–116 m were F36A and Y68A.

Cell culture, transfections, RNAi and protein overexpression

HeLa and PAC-1 cells were grown in Dulbecco's modified Eagle's medium supplemented with Glutamax (Invitrogen) and 10% Fetal bovine serum (FBS). Transient transfections were carried out in 6-well dishes seeding 10^5 cells per well 24 h before transfection. Transfections were set-up in quadruplex; one set for western analysis and three for RT–PCR. For each well, 1 μg of DNA was pre-incubated with 3 μl (HeLa cells) or 6 μl (PAC-1 cells) of Lipofectamine (Invitrogen) for 30 min in 200 μl of Opti-Minimal essential medium (MEM) I before making the volume up to 1 ml and adding to cells that had been pre-washed with Opti-MEM I. The DNA Lipofectamine complex was left on the cells for 5 h before being replaced with fresh medium. Cells were harvested 48 h after transfection. For RNAi, a 4-day two hit protocol was followed whereby the cells were seeded at 2×10^5 per well in 1.7 ml of medium. After 7 h, 15 μl of Oligofectamine (Invitrogen) was pre-incubated for 5 min with 60 μl Opti-MEM I and then added to 250 μl Opti-MEM I containing MBNL1-specific THH2 siRNA (30) to a final concentration of 10 nM. For PAC-1 cells, a MBNL2-specific siRNA was also included at 10 nM (Dharmacon GAAGAGUAAUUGCCUGCUUUU).

This was complexed for 20 min and added directly to the medium. When carrying out a knockdown together with overexpression 16 h after the first hit, the cells were transfected as aforementioned using Lipofectamine. Five hours later, the medium on the cells was replaced with 1.5 ml of Dulbecco's modified Eagle's medium containing 10% FBS. A second hit was carried out using 3 µl of Lipofectamine 2000 together with a final concentration of 10 nM MBNL1 (plus 10 nM MBNL2 for PAC-1 cells)-specific siRNA in 0.5 ml of Opti-MEM I, complexed for 20 min and then added directly to the cells. Cells were harvested 48 h after transfection.

pEGFP–MBNL1 293 T nuclear extracts were made by transfecting 5- × 150-cm plates at a cell density of 3.6×10^6 cells per plate with 18 µg of DNA. Cells were harvested after 36 h, and nuclear extracts were prepared as previously described (46). Nuclear extracts were also prepared from HeLa S3 suspension cells or PAC-1 cells.

Expression of pCGTHCF$_{FL}$T7 MBNL1 for recombinant protein was carried out transiently in 293T cells. Four 150-cm plates were seeded with 8×10^6 cells per plate 24 h before transfecting with 54 µg of DNA together with 72 µl of Lipofectamine 2000 following Invitrogen protocol. DNA complexed with Lipofectamine was left on the cells for 48 h before harvesting. Proteins were bound to T7 Tag antibody agarose (Novagen) and purified according to the manufacturer's instructions (43).

Recombinant pQE–PTB1 and pQE–PTB4 were prepared as previously described (19). Recombinant GST-tagged MBNL1 clones amino acids 2–253, 2–116, 2–91, 2–72 and GST–Sxl were all purified using Glutathione Sepharose 4B according to the manufacture's protocols. MBNL1 amino acids 2–253 protein was further purified on either Mono Q or HiLoad Superdex 75 columns.

RT–PCR and western analysis of transfections

Total RNA was isolated using TriReagent (Sigma). The RNA was resuspended in 90 µl of water and treated with 2 U of DNase I (Ambion) in 10 mM Tris, pH 7.5, 2.5 mM $MgCl_2$ and 0.5 mM $CaCl_2$. The RNA was phenol extracted and ethanol precipitated. One micrograms of RNA was annealed with 100 ng of SV3′RT primer at 55°C for 15 min before incubating together with 10 U of Avian Myeloblastosis Virus (AMV) reverse transcriptase in 50 mM Tris, pH 8.3, 40 mM KCl, 8 mM $MgCl_2$, 2 mM dithiothreitol (DTT) and 1 mM dNTP at 42°C for 1 h. For the PCR, 2 µl of RT was mixed with 25 pmol SV5′2 in 50 mM KCl, 10 mM Tris, pH 8.3, 2.5 mM $MgCl_2$, 0.001% (w/v) gelatin and 0.2 mM dNTP and heated to 92°C for 3 min before cooling to 80°C on which the remainder of the reaction was assembled by adding 4 pmol ^{32}P γ ATP end-labelled SV3′1 with 1.25 U of Taq polymerase. Thirty cycles, 94°C for 30 s, 62°C for 30 s and 72°C for 60 s, were carried out followed by a final extension of 72°C for 2 min. One microlitre of the PCR was diluted into 20 µl of formamide, 10 mM EDTA, 0.1% bromophenol blue, 0.1% xylene cyanol and 5 µl run on a 4% denaturing PAGE. Oligonucleotides for RT–PCR were:

SV3′RT: 5′-GCAAACTCAGCCACAGGT-3′
SV5′2: 5′-GGAGGCCTAGGCTTTTGCAAAAAG-3′
SV3′1: 5′-ACTCACTGCGTTCCAGGCAATGCT-3′

Quantitation of RT–PCR data represents the mean ± standard deviation of at least three biological replicates carried out at the same time. Because of the variable phenotype of PAC1 cells, there is some minor variability between absolute values for identical experiments carried out at different times; however, the relative differences between different constructs are always maintained (e.g. lanes 1–4 of Supplementary Figure S3B and C).

For western blots, cells were washed twice with phosphate-buffered saline (PBS), and 100–150 µl of 2× SDS loading buffer, pre-heated to 90°C, was added directly to the cells. Using the flat end of a P1000 tip, the cells were vigorously disrupted and then transferred to an Eppendorf and immediately frozen on dry ice. The samples were heated to 90°C for 5 min and frozen a second time on dry ice. They were either stored at −20°C for later use or reheated to 90°C for 5 min before loading onto a 15% Laemelli gel. Proteins were transferred onto Millipore nylon membrane by western blotting and blocked in 4% Marvel TBST overnight at 4°C. Blots were probed using standard protocols using Enhanced chemiluminescence (ECL). Primary antibodies used were anti-actin (Sigma, A2066), anti-green fluorescent protein (GFP) (Molecular Probes, A11122), anti-FLAG M2 (Sigma, F1804), anti-MBNL1 (Sigma, M3320), anti-MBNL2 H-81 (Santa Cruz, sc-134813), anti-hnRNP C 3G6 (Santa Cruz, sc-32315, gift from J. Ule), anti-hnRNP H (gift from D. Black), hnRNP L N-15 (Santa Cruz, sc-30720), anti-GST-2 (Sigma G1160), anti-PTB and anti-MS2 (in-house rabbit polyclonal antibody).

In vitro transcription and UV cross-linking

High-specific activity [α-^{32}P] UTP-labelled RNA probes of the *Tpm1* regulatory elements were made by standard methods using either T7 or SP6 RNA polymerase. A total of 10 fmol of full-length RNA with all the *cis*-regulatory elements, 20 fmol of P3 or DY element and 50 fmol of U or D elements were incubated in 10-µl reactions containing 10 mM HEPES, pH 7.9, 3 mM $MgCl_2$, 5% glycerol, 1 mM DTT, 100 mM KCl and 50 µg/ml of rRNA with either 0.024 µM rMBNL1, 0.25 µM rPTB4 or 0.5 mg/ml HeLa nuclear extract for 25 min at 30°C. Heparin, 2.5 mg/ml, was added for 5 min, and the sample UV cross-linked in a Stratalinker using 1920 mJ. The reaction was incubated for 30 min at 37°C together with 0.27 mg/ml of RNase A1 and 0.75 U/ml RNase T1. Four microlitres of a 4× SDS loading buffer was added to each reaction, the samples heated to 90°C for 5 min and then loaded on a 15% Laemelli gel. The sequences of SELEX RNAs were: MBNL D12 (40) 5′-GGGAGACA AGCUCCUCCUGCGCUCUUUGCUUGCCCUGCU GUGUCGAAUU-3′, PTB 5′-GGGAGACAAGCUUC [CUCUU]$_6$GAAUU-3′.

In vivo IP

In vivo formaldehyde cross-linked protein lysates were made from two 15-cm plates. Transfected cells

were washed in PBS and then left in 20 ml of PBS until the cells floated off the plate and transferred to a tube. Formaldehyde was added to 0.4% and left for 10 min on the bench. Cell pellets were washed with PBS and resuspended in 100 µl per 10^7 cells of 50 mM Tris, pH 7.5, 150 mM NaCl, 50 µM $ZnCl_2$, 2.5 mM $MgCl_2$, 5% glycerol, 0.5% NP-40, 1 mM PMSF, protease inhibitor cocktail (Roche) and 25 U/ml of Benzonase (Novagen), left on ice for 30 min and centrifuged at 14 000 rpm for 5 min at 4°C. The supernatant was transferred to a fresh tube.

Total protein lysate (50–100 µg) was immunoprecipitated with 12 µg of anti-FLAG M2 antibody in 1 ml of 50 mM Tris, pH 7.5, 150 mM NaCl, 1 mM EDTA and 1% Triton X-100, rotating at 4°C for 2–3 h. Fifty microlitres of protein G Dynabeads were added for 1 h further. The samples were washed once with the binding buffer and twice with PBS. The proteins were eluted off the beads using 60 µl of 3× FLAG peptide at 250 ng/µl (Sigma F4799). Twenty-five per cent of the pull-down was loaded on a gel for western blot.

Anti-GFP immunoprecipitation was carried out with GFP-Trap-M beads (Chromotek). Twenty-five microlitres of protein lysates were incubated with 15 µl of magnetic beads in 1 ml of 50 mM Tris, pH 7.5, 500 mM NaCl, 0.5 mM EDTA, 0.05% NP-40, 1% Tween-20, 5% glycerol, 1 mM PMSF and protease inhibitor cocktail for 1.5 h rotating at 4°C. The magnetic beads were washed three times with 1 ml of 20 mM Tris, pH 8, 800 mM NaCl, 2 mM EDTA, 1% Triton X-100, 0.5% SDS, 5% glycerol, 1 mM PMSF transferring to a fresh tube on the last wash. The beads were resuspended in 50 µl of SDS loading buffer, heated for 10 min at 90°C and 20 µl loaded on a gel for western blot.

Total internal reflection fluorescence analysis

Single molecule experiments we carried out as described previously (20) with minor modifications. Briefly, for RNA labelling, an oligonucleotide ATTO 647 N-5′-TUGUCUCCCAU-3′–biotin (complementary to the first 9 nt of either RNA) was used (Eurogentec, Belgium), where the underlined bases are locked nucleic acid (LNA) bases and the others are 2′OMe bases. RNA (50 nM) was incubated with either GFP–PTB or GFP–MBNL1 overexpressed nuclear extracts (50%, 10 µl of incubation volume) at 30°C for 30 min, then the mixture was diluted 10 000- to 50 000-fold, and 25 µl of this diluted mixture was injected into the microscope chamber. Acquisitions were recorded for 500 time bins (200 ms/bin) starting with ATTO 647 N (633-nm laser excitation) for 30 bins with the rest for GFP (488-nm laser excitation, 13–15 mW of laser power at the prism) recording the split signal from each colour on the corresponding half of the emCCD (iXon DV887, Andor) chip. In all, 20–25 acquisitions were recorded for each experiment. Time series intensities for co-localized spots were extracted from 10×10 pixel areas and background corrected. Incubations without RNA were analysed in a similar manner and used to extract the data for behaviour of individual GFP molecules (bleaching, total emission) showing the presence of ~10% (GFP–MBNL nuclear extract) or ~15% (GFP–PTB nuclear extract) two-step bleached spots. Average detected emissions from single fluorophores (GFP–MBNL and GFP–PTB) were calculated by exponential approximation of the cumulative distribution of detected photons corrected for the presence doubles (they were similar for both nuclear extracts). The number of bound proteins for each experiment was estimated from the analysis of both distribution of bleaching steps and cumulative distribution of detected emissions (20) with corrections for the presence of doubles.

FRET/FLIM

HeLa cells were plated onto coverslips pre-treated with 1 µl Cell-Tak (BD Biosciences) and transfected with 0.5 µg of plasmid in 25 µl Opti-MEM I (Invitrogen) using Fugene HD (Roche Diagnostics) according to manufacturer's protocol. Approximately 24 h after transfection, cells were fixed for 10 min in 4% formaldehyde containing PBS at 37°C, washed several times with PBS and finally mounted with Mowiol mounting medium.

A detailed description of the FLIM instrument, FRET measurements and analyses can be found elsewhere (47). Briefly, the Venus samples were excited at 485 nm by a frequency-doubled short laser pulse from a Chameleon XR Ti:Sapphire Laser (Coherent) tuned at 970 nm. Images were recorded on a Zeiss Axiovert S100TV with a 63× 1.4 NA oil immersion objective through a 495LP dichroic mirror (AHF, Germany) and a BL HC536/40 emission band-pass filter (AHF, Germany) with an intensified PicoStar HR 12 CCD camera system (LabVision, Germany). Images were acquired and analysed with self-written software (LabView 8.2, National Instruments). The fluorescence decay curves were recorded with 16 images with increasing delay times (step 500 ps) after the excitation laser pulse with a camera binning of 2×2 and an exposure time of 100–200 ms for each image. The laser power was adjusted by ND filters to avoid photobleaching during the acquisition. Finally, images were background corrected, and the fluorescence lifetime was calculated for each pixel according to:

$$I = A \cdot e^{-t/\tau}$$

with I the measured intensity in each pixel at a time-point t, the pre-exponential factor A and fluorescence lifetime τ.

GST pull-down assay

GST pull-down assays have been previously described (23). The buffer was modified to include 50 µM zinc chloride. Pull-downs in HeLa nuclear extract used 50 µg of protein with 1 µg of GST-tagged protein. RNase A and T1 were added at 0.1 mg/ml and 1000 U/ml, respectively. The RNA was titrated up to a 20 M excess over the GST protein. Recombinant protein only pull-downs included a 1.75 M excess of pQE–PTB4 over GST–MBNL1 amino

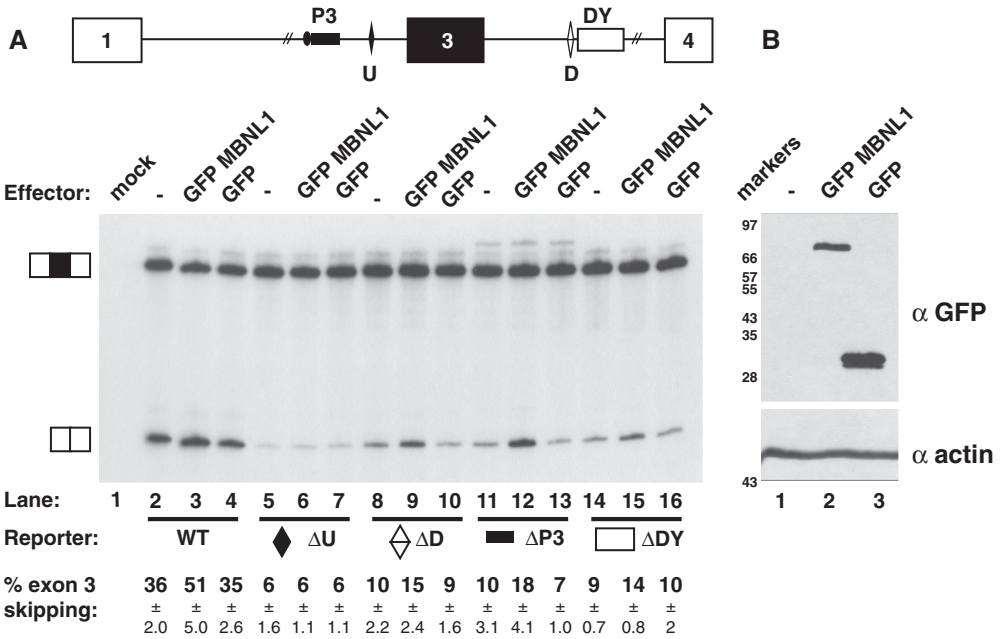

Figure 2. The upstream UGC element mediates effects of overexpressed MBNL1. (**A**) RT–PCR analysis of PAC-1 cells transfected with minigenes that are wild-type (WT), lanes 2–4, or have a deletion of upstream UGC element (ΔU) lanes 5–7, a deletion of the downstream UGC element (ΔD) lanes 8–10, point mutations of the UCUU motifs in exon 3 polypyrimidine tract (ΔP3) lanes 11–13 or a deletion of downstream UCUU element (ΔDY) lanes 14–16, were expressed alone or together with GFP–MBNL1 or GFP. Lane 1, mock control. (**B**) Western blot analysis showing overexpressed GFP–MBNL1 or GFP with actin as a loading control.

acids 2–253 and included a 0.01:1, 0.1:1 and 1:1 M ratio of RNA to GST protein.

RESULTS

MBNL proteins regulate *Tpm1* splicing

In view of the potential MBNL motifs in the U and D elements flanking *Tpm1* exon 3 (Figure 1A), we decided to test whether MBNL proteins regulate splicing of this exon. We knocked down MBNL1 and MBNL2 individually in the PAC1 rat pulmonary artery smooth muscle cell line in which *Tpm1* splicing is regulated (13). Despite ~75% decreases in MBNL levels (Figure 1B, lanes 5–7), the effects on *Tpm1* splicing were minimal (Figure 1C). However, as observed by others (39), individual knockdown of MBNL1 or 2 is associated with an increase in the levels of the other family member (Figure 1B, lanes 5–7), which may mask downstream consequences. Consistent with this, combined *MBNL1* and *2* knockdown (Figure 1B, lane 8) led to increased *Tpm1* exon 3 and decreased exon 2 inclusion (Figure 1C). This indicates that selection between the *Tpm1* exons 2 and 3 is regulated by MBNL proteins. To address whether this regulation involves repression of exon 3, we transfected PAC1 cells with a minigene construct lacking exon 2, but in which exon 3 is skipped in smooth muscle cells (14,18). Skipping of exon 3 was reduced from 26 to 8% on *MBNL1/2* knockdown, and this effect was fully reversed by overexpression of siRNA-resistant human MBNL1 fused to Venus fluorescent protein (Figure 1D, left panel). We also tested the ability of a series of MBNL1 deletion mutants to complement the *MBNL1/2* knockdown. A protein retaining the N-terminal ZF domains (amino acids 2–253) but lacking the C-terminal region retained ~30% of full length (FL) activity, whereas all further deletions of ZF3 and 4 and the linker between ZF 2 and 3 lost all activity. Likewise, an N-terminal deletion mutant lacking the ZF1–4 but retaining the C-terminal region was completely inactive.

We also tested the activity of MBNL1 in HeLa cells using a *Tpm1* minigene in which exon 3 skipping is increased by a mutation of its branch point (construct pTΔBP) (42). Control experiments established that the elevated levels of exon skipping in HeLa cells remained dependent on the known regulatory elements (Supplementary Figure S1). In contrast to PAC1 cells, knockdown of MBNL1 alone was sufficient to cause changes in splicing, consistent with previous reports (30). Exon 3 skipping in the pTΔBP construct was reduced from 53 to 22%, and this effect was fully reversed by co-transfection of MBNL1–GFP (Figure 1D, right panel). MBNL proteins, therefore, act as repressors of *Tpm1* exon 3 in PAC1 and HeLa cells.

We next tested whether the activity of MBNL proteins on *Tpm1* exon 3 was mediated by the known silencer elements (14,16–18). We co-transfected GFP–MBNL1 or GFP expression vectors into PAC-1 cells along with reporter constructs with deletions of either the upstream (ΔU) or downstream (ΔD) UGC elements, the downstream pyrimidine tract (ΔDY), or point mutations of the PTB-binding sites in the polypyrimidine tract of exon 3 [ΔP3 (23,44)] (Figure 2). The wild-type construct showed 36% exon skipping, which was elevated to 51% by

GFP–MBNL1 but not GFP (Figure 2A, lanes 2–4). As expected, exon skipping was reduced to between 6 and 10% by each of the regulatory element mutations (compare lane 2 with lanes 5, 8, 11 and 14). However, with the exception of the ΔU deletion mutant (lanes 5–7), each of the regulatory element mutants remained responsive to GFP–MBNL1 overexpression. This suggests that the U element is critical for mediating the effects of overexpressed MBNL1.

UGC elements bind MBNL proteins

To address whether MBNL1 affects *Tpm1* splicing directly we carried out UV cross-linking of *in vitro* transcribed *Tpm1* RNA to recombinant MBNL1 and to proteins in PAC1 nuclear extract. Wild-type RNA, with all four *cis*-regulatory elements intact, cross-linked to rMBNL1 (Figure 3B lane 1, RNA 'a'). In PAC1 NE, it cross-linked to proteins of ~59, 57, 45 and 35 kDa. The 59/57 kDa doublet was shown by immunoprecipitation to be PTB (Figure 3B, lane 13), whereas the ~44 kDa band was MBNL1 (lane 10). As expected, deletion of the DY element together with point mutations of UCUU motifs in P3 (RNA 'c') led to reduced PTB cross-linking (lanes 6 and 15) (17,18,20), but it had no effect on MBNL1 cross-linking (lane 3, 6, 9 and 12). Conversely, combined deletion of the U and D elements (RNA 'b') substantially reduced cross-linking of both recombinant (lanes 2 and 8) and NE MBNL1 (lanes 5 and 11), indicating that these are the major sites of MBNL1 interaction. The cross-linking of PTB also seemed to be slightly reduced by the combined U/D element mutations in RNA (lanes 5 and 14, see later in the text). To test whether the U or D elements are sufficient for MBNL1 binding, we used RNAs e and f for UV cross-linking (Figure 3A). MBNL1 cross-linked to both the U and D elements (Figure 3C, lanes 3 and 4). In contrast, recombinant PTB bound to the pyrimidine tract elements (RNAs d and g, lanes 7 and 10) but not to the UGC elements (lanes 8 and 9). Although only the U element was essential for mediating the influence of overexpressed MBNL1 (Figure 2), both the U and D elements can bind MBNL1 (Figure 3C). Indeed, the D element cross-linked more efficiently than the U element (Figure 3C, lanes 3 and 4).

We next used single molecule total internal reflection fluorescence (TIRF) microscopy (20) to examine the interaction of MBNL1–GFP with wild-type *Tpm1* RNA (RNA a from Figure 3), and RNAs with mutations in all the known PTB-binding sites (RNA c) or MBNL1-binding sites (RNA b′). RNA b′ contained deletions of the U and D elements and point mutations in two additional YGCY motifs upstream of exon 3. The mutations of the additional motifs reduce exon 3 skipping, although the effect is much less than with the ΔU or ΔD deletions (Supplementary Figure S3). As previously described (20), nuclear extracts from HEK293T cells expressing GFP–MBNL1 were incubated with RNA pre-annealed to biotinylated oligonucleotide that was coupled with ATTO 647N dye, and the mixtures were diluted and immobilized on a silica slide. There was clear evidence for multiple (~3–8) binding events from multiple bleaching steps that were seen on the time traces of detected emissions and from the cumulative distributions of total photon emissions, but we were unable to determine unambiguously the stoichiometry of MBNL1–RNA interactions. The percentage of RNA spots co-localizing with labelled proteins gives an indication of the apparent affinity of interaction between the labelled protein and RNA (20). Wild-type RNA a and the PTB site mutant RNA c showed 17% co-localization with GFP–MBNL, which was reduced to 8% with the MBNL-binding site mutant RNA b′ (Table 1). These results confirm that the interaction of MBNL1 with *Tpm1* RNAs involves the identified U and D elements. Moreover, we conclude from the experiment with RNA c that the binding of PTB does not contribute significantly to MBNL1 association.

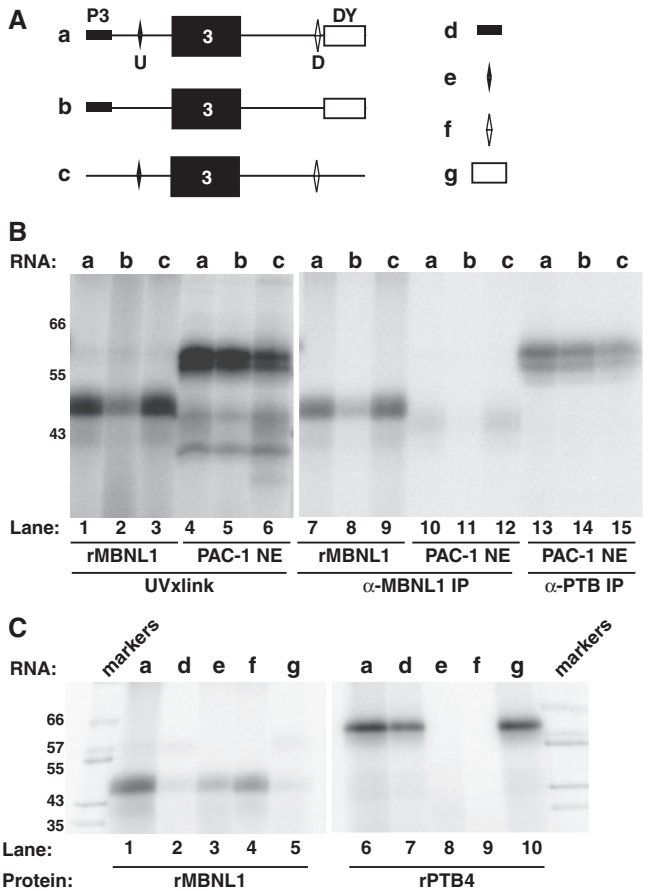

Figure 3. MBNL binds to the upstream and downstream UGC elements. (**A**) Schematic representation of RNAs a–g containing *Tpm1* exon 3 and flanking regulatory elements. RNA a has all the *cis*-elements, RNA b has the UGC motifs deleted and RNA c has the UCUU motifs mutated in P3 or deleted in DY. RNAs d–g contain the individual regulatory elements as indicated. (**B**) *In vitro* transcribed RNAs a–c were UV cross-linked with either recombinant pCGT7–MBNL1 (rMBNL1, lanes 1–3) or PAC-1 nuclear extract (NE, lanes 4–6). RNAs a–c were UV cross-linked with rMBNL1 or PAC-1 nuclear extract and then immunoprecipitated with either α-MBNL1 (lanes 7–12) or UV cross-linked with PAC-1 nuclear extracts and immunoprecipitated with α-PTB antibody (lanes 13–15). (**C**) *In vitro* transcribed RNA a or the individual *cis*-elements, d–g, were UV cross-linked with rMBNL1 (lanes 1–5) or recombinant pQE–PTB4 (rPTB4, lanes 6–10).

Table 1. Co-localization of *Tpm1* RNA with GFP-tagged MBNL1 and PTB determined by single molecule TIRF microscopy

Nuclear extract	RNA	Binding sites mutated	Proportion of co-localized spots	Total co-localized spots	Total red (RNA) spots
MBNL–GFP	a	None	0.17	583	3456
	b′	MBNL	0.08	142	1750
	c	PTB	0.17	129	752
PTB–GFP	a	None	0.66 [a]		
	b′	MBNL	0.39	907	2352
	c	PTB	0.42	149	355

RNA species a and c referred to as TM1 and TM4 in Cherny *et al*. (20). RNA b′ identical to RNA b in Figure 3, with the two additional mutations (CGCU to CCCU and UGCC to UCAC) indicated in Supplementary Figure S3.
[a]Value for RNA a with PTB–GFP taken from previous studies (17–20).

To determine whether MBNL-binding sites affect the binding of PTB, we analysed the interaction of the three *Tpm1* RNAs with GFP–PTB. As previously observed, mutation of the PTB-binding sites reduced the degree of co-localization of GFP–PTB with *Tpm1* RNA from 66 to 42% (compare RNAs a and c, Table 1), and the number of PTB molecules bound was reduced from 5–6 to 3–4. The MBNL-binding site mutant RNA b′ also bound 5–6 GFP–PTBs, consistent with the fact that the PTB-binding sites had not been targeted. However, the degree of co-localization was only 39%, indicating that mutation of the MBNL1-binding sites reduces the apparent affinity of PTB binding to its sites on *Tpm1* RNA, without altering the number of PTB sites. We conclude that MBNL1 contributes to the recruitment of PTB, but PTB does not contribute to the binding of MBNL.

Artificially tethered MBNL1 is active at U and D locations

Having shown that recombinant MBNL1 can bind to both the UGC elements, we next used an artificial tethering system. The logic of this approach is to substitute a protein-binding RNA element with a binding site for MS2 bacteriophage coat protein, leading to loss of regulatory function. If a fusion of MS2 coat protein to the original RNA-binding protein restores function, this demonstrates that the precise nature of the RNA–protein recognition is not crucial for function, and it allows deletion mapping of effector domains. We have used this system previously to define domains of PTB and Raver1 sufficient for inducing skipping of *Tpm1* exon 3 (24,45).

Replacement of the D element by two MS2 sites led to a reduction of exon skipping in PAC 1 cells to 7% (Figure 4B, lane 2). Full-length MBNL1–MS2 led to an increase in exon skipping to 57%, whereas co-transfection with MS2 was without effect (lanes 3 and 11). Control experiments showed that MBNL1 alone produced a much smaller effect than MBNL1–MS2 (Supplementary Figure S3B, lanes 6 and 10). Thus, artificial recruitment of MBNL1–MS2 compensates for deletion of the D element. We next tested a series of C-terminally truncated MBNL1 mutants fused to MS2, as well as an N-terminal deletion mutant lacking the four ZF domains (Figure 4B), all of which were expressed to similar levels (Figure 4D, left panel). To facilitate comparison of the effects of deletion mutations in different contexts, we calculated the activity of mutants as a percentage of the exon skipping caused by full-length MBNL1–MS2 compared with MS2 alone (numbers with black background in Figure 4B and C). This value is not corrected for the residual activity of untethered MBNL proteins (Supplementary Figure S3), but only the full-length protein and the 2–253 mutant showed any activity in an untethered assay (Figure 1D). The C-terminal deletion mutant containing all four ZFs (amino acids 2–253) retained 83% of full-length activity, whereas ZF1 and 2 and the complete following linker region (amino acids 2–183) retained 78% of full-length activity (lanes 4 and 5). Further deletions removing the linker region between ZF2 and 3 reduced activity progressively (lanes 5–9), with amino acids 2–72 having only 8% activity. An N-terminal deletion mutant lacking all ZFs (amino acids 239–382) had 34% of full-length activity (lane 10).

Replacement of the U element by an MS2 site led to a reduction in exon skipping in PAC1 cells to ~9% (Figure 4B, lane 13) and co-transfection with MS2 alone reduced this slightly (lane 22). Overexpression of full-length MBNL1–MS2 increased exon 3 skipping to 52% (lane 14). Control experiments showed that MBNL1 alone produced a much smaller effect than MBNL1–MS2 (Supplementary Figure S3C, lane 9 compared with lane 6), in contrast to the ΔU construct (Figure 2), which showed no response to MBNL1 overexpression. Compared with tethering at the D location, all of the deletion mutants showed substantially greater impairment of activity at the U location, with only 2–253 retaining >50% activity (Figure 4B, lanes 15–21).

We carried out similar MS2 tethering experiments in HeLa cells by substituting the U and D elements with MS2 sites in the background of the mutated branch point minigene, pTΔBP which shows ~50% exon 3 skipping in HeLa cells (Supplementary Figure S1). Replacement of the D element by two MS2 sites led to a reduction in exon skipping to 18%, which was reduced further to 11% by expression of MS2 protein (Figure 4C, lanes 2 and 11). Tethering of full-length MBNL1 led to 73% exon skipping and the N-terminal region (amino acids 2–253) retained 89% of this activity (Figure 4C, lanes 3 and 4). Further C-terminal deletions had lower activity, but all mutants with additional linker sequences upstream of ZnF 2 retained 60–70% activity of full-length MBNL1–MS2 (lanes 4–8). The minimal ZnF1

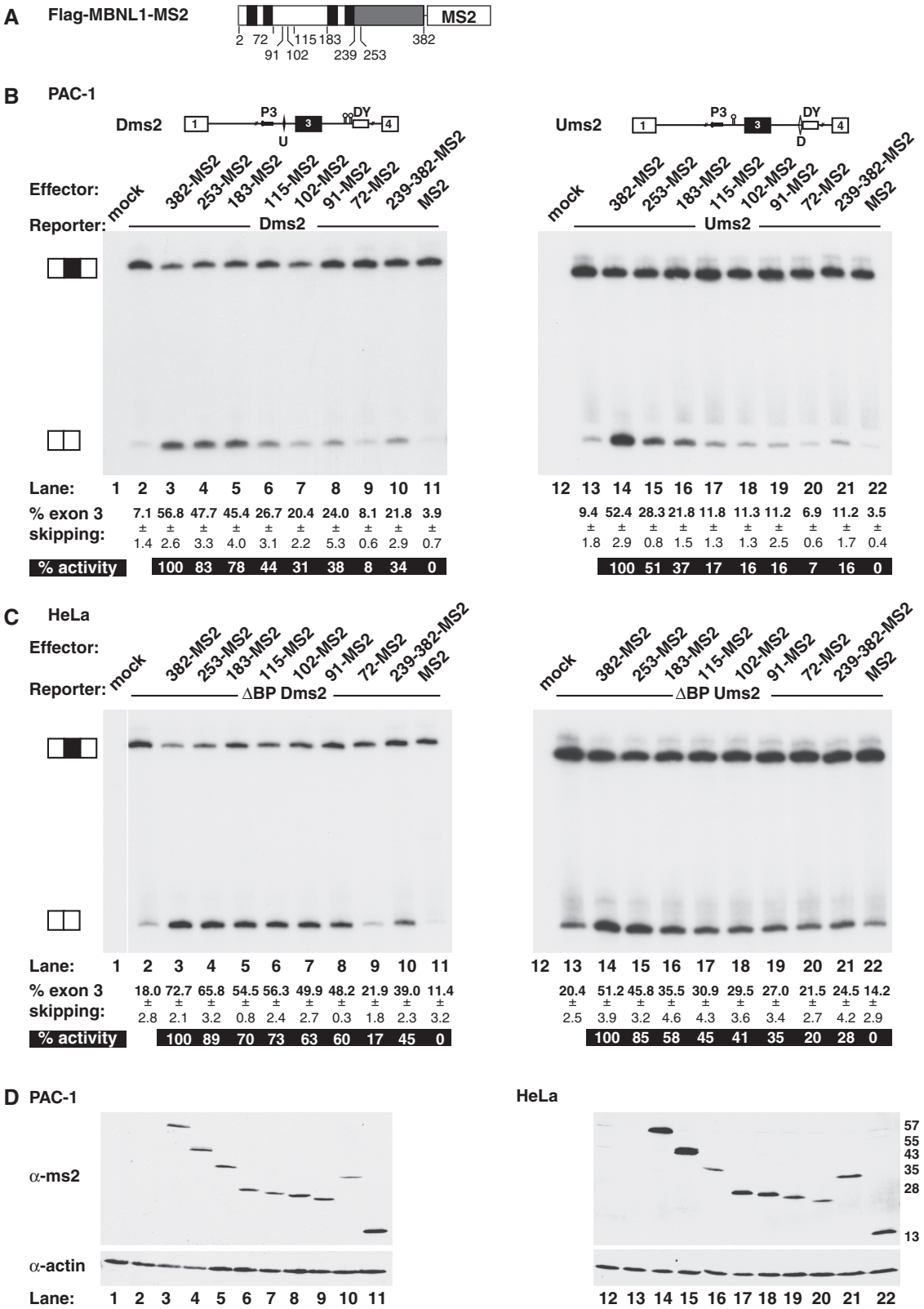

Figure 4. MS2 tethering of MBNL1 promotes exon 3 skipping. (**A**) Schematic representation of FLAG-tagged MBNL1–MS2 fusion proteins. All C-terminal truncations start at amino acid 2 and are full-length (382–MS2), 2–253 (253–MS2), 2–183 (183–MS2), 2–115 (115–MS2), 2–102 (102–MS2), 2–91 (91–MS2) and 2–72 (72–MS2), with a C-terminal fragment amino acids 239–382 (239–382–MS2). The black boxes represent the four ZF domains; the grey shaded box represents the C-terminus. The MS2 coat protein is at the C-terminus and the FLAG tag at the N-terminus. (**B**) A schematic representation of the *Tpm1* minigenes used for recruitment of MS2-fused MBNL1 truncations in PAC-1 cells. Two MS2 hairpins were used to replace the D element (Dms2) and one MS2 hairpin to replace the U element (Ums2). RT–PCR analysis of the MS2 minigene reporters, lanes 2 and 13. Lane 3–11 and 14–22 overexpressed full-length MBNL1–MS2 (382–MS2), amino acids 2–253–MS2 (253–MS2), 2–183–MS2

(continued)

and 2 fragment (amino acids 2–72) had only 17% activity (lane 9). The C-terminal region amino acids 239–382 (lane 10) was more active than the minimal ZnF1 and 2, but less active than all other constructs. All deletion mutants were detectably expressed in HeLa cells, albeit with some variability in levels (Figure 4D, right panel).

Replacement of the U element by an MS2 site led to reduction in exon skipping to 20% in HeLa cells, and this was further reduced to 14% by MS2 (Figure 4C, lanes 13 and 22). Overexpression of full-length MBNL1–MS2 increased exon skipping to 51% (lane 14) and deletion of the C-terminal region had little effect (lane 15). Further C-terminal truncations progressively lost activity (lanes 15–20).

The preceding data show that the functional effects of deleting either the upstream or downstream UGC element could be reversed by artificial recruitment of full-length MBNL1. The effects of deletions varied according to the location of recruitment and between PAC1 and HeLa cells, with deletions being more tolerated in the D than the U location, and in HeLa cells than in PAC1 cells (Supplementary Figure S4). However, in all cases, the N-terminal region containing the ZFs had much higher activity than the C-terminal region. Furthermore, regions of MBNL1 containing just the first two ZFs and the following linker region retained substantial activity, suggesting that this part of MBNL1 is critical for its activity.

MBNL1 interacts with PTB

The U and D regulatory elements are both located adjacent to pyrimidine tracts that can bind 2 or 3 PTB molecules, which repress splicing (18,20). Moreover, the TIRF analyses indicated that the U and D elements increased the apparent affinity of PTB for *Tpm1* RNAs (Table 1). Although both proteins have been studied extensively, there have been no previous reports of a direct interaction between them. Co-immunoprecipitation experiments using various epitope-tagged PTB and MBNL1 combinations produced negative results (data not shown). To address whether PTB and MBNL1 interact in a manner that is unstable during cell lysis and immunoprecipitation, we co-transfected HeLa cells with FLAG–PTB and Venus–MBNL and then treated cells with formaldehyde to induce protein–protein cross-links. After anti-FLAG immunoprecipitation and cross-link–reversal, western blots were probed with PTB and GFP antibodies (Figure 5B). Full-length Venus–MBNL and all members of a C-terminal deletion series were pulled down along with FLAG–PTB (Figure 5B, lanes 11–17); indeed, the mutants lacking the C-terminal region were pulled down with greater efficiency. In contrast, the C-terminal fragment of MBNL1 (amino acids 239–382), which lacks the ZnF domains (lanes 1–9), showed background levels of pull-down (lane 18). These data suggest that MBNL1 and PTB are associated together in the cell. To pursue this further, we analysed cells transfected with mCherry-tagged PTB and Venus-tagged MBNL1 by fluorescence lifetime imaging Förster resonance energy transfer (FLIM–FRET, Figure 5C and D). Transfection of either Venus–MBNL or mCherry–PTB showed both proteins to be nuclear localized with additional cytoplasmic signal for Venus–MBNL (Figure 5C). If the two proteins interact, energy transfer from Venus to mCherry should reduce the fluorescence lifetime of Venus. Indeed, the lifetime of nuclear, but not cytoplasmic, Venus–MBNL1 or MBNL1–Venus was reduced on co-transfection with mCherry–PTB (Figure 5C, panels a and b), indicating a direct interaction between MBNL1 and PTB. The reduction in fluorescence lifetime was also observed with the N-terminal but not the C-terminal region of MBNL1 (Figure 5C, panels c and d), consistent with the pull-down data (Figure 5B). Thus, the FLIM–FRET data indicated that the N-terminal region (amino acids 2–253) of MBNL1 is involved in interaction with PTB, whereas the cross-link–immunoprecipitation (IP) suggested amino acids 2–72 may be sufficient.

We next asked which region(s) of PTB were involved in the interaction (Figure 6) by the cross-link co-immunopreciptation approach using full-length Venus–MBNL1 and FLAG-tagged PTB deletion mutants. Pull-down was carried out with GFP–TRAP beads and western blots with anti-GFP and anti-FLAG (Figure 6B). Venus–MBNL1 pulled down full-length PTB (Figure 6B, lane 10), as well as the N-terminal part of PTB containing RRM domains 1 and 2 and following linker (lane 11). However, RRM2 and the following linker (2L, lane 12) or RRMs 3 and 4 (lane 13) were not pulled down. Similar results were seen by FLIM–FRET (Figure 6C and D); the fluorescence lifetime of nuclear Venus–MBNL1 was reduced by mCherry–PTB or Cherry–PTB-12L, but not by mCherry–PTB-34 (Figure 6C and D).

Taken together, the data of Figures 5 and 6 indicate that MBNL1 and PTB interact with each other via their N-terminal regions. Strikingly, these are the same parts of the two proteins that act as repressor domains when artificially tethered [Figure 4; (45)]. However, the requirement for cross-linking to detect the interaction by co-immunoprecipitation suggested that the interaction might be weak. Moreover, the fact that interacting parts of both proteins minimally involved 2 RNA-binding domains within each protein, suggested that the interaction might be RNA-dependent.

RNA binding by MBNL1 promotes interaction with PTB

To further investigate the role of RNA in the PTB–MBNL1 interaction, we purified recombinant GST

Figure 4. Continued
(183–MS2), 2–115–MS2 (115–MS2), 2–102–MS2 (102–MS2), 2–91–MS2 (91–MS2), 2–72–MS2 (72–MS2) and MS2 only, respectively. Lanes 1 and 12 are mock transfected cells. The '% activity' (white text on black background) was calculated from the difference in percentage of exon skipping between MS2 alone and each construct, normalized to the response of full-length 382–MS2 as 100%. (**C**) MS2 recruitment in HeLa cells as in (**B**) using reporter minigene with the branch point mutation (pTΔBP). (**D**) Western blot analysis using anti-MS2 antibody to detect overexpressed MBNL1 and anti-actin as a loading control in PAC-1 cells (left panel) and HeLa cells (right panel).

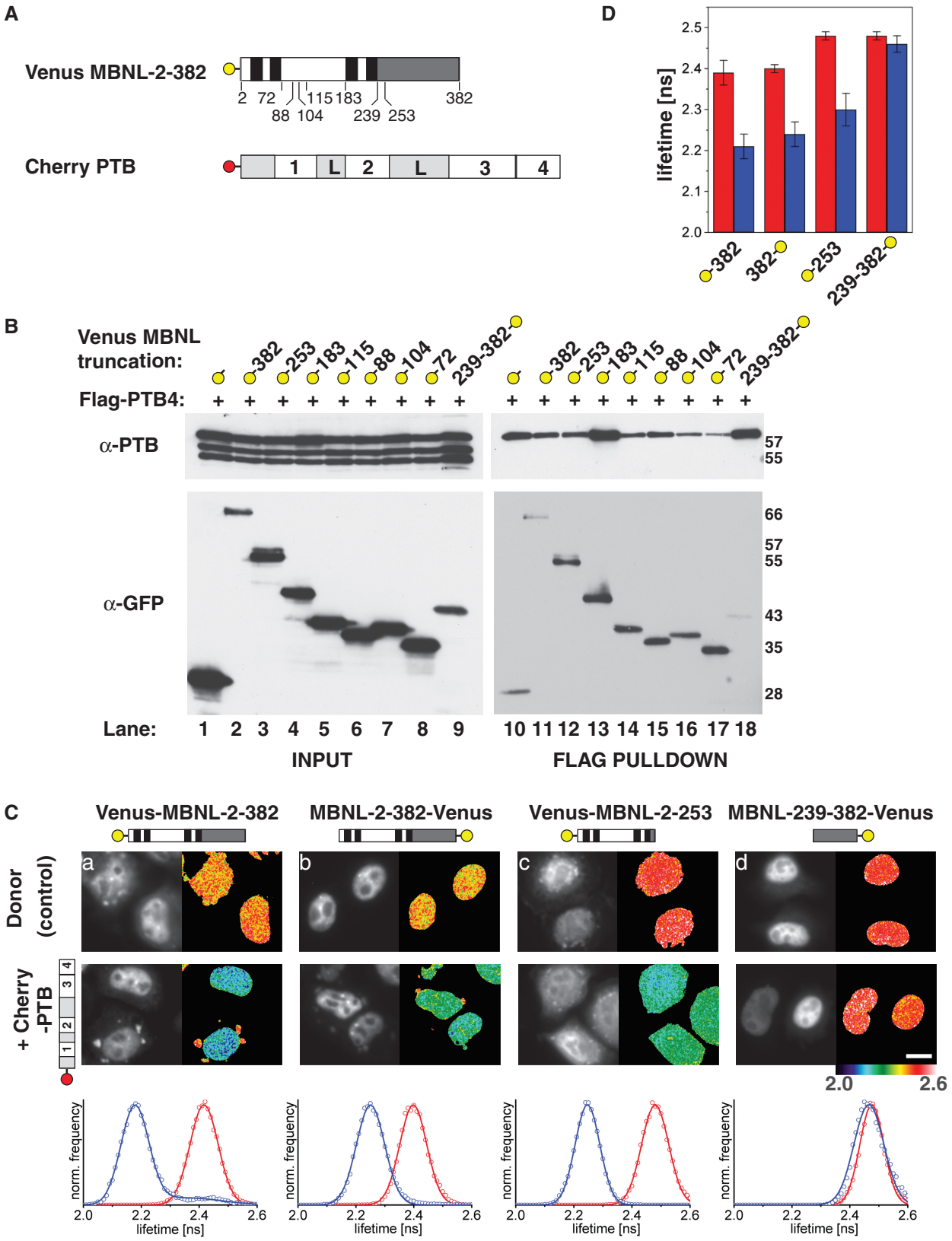

Figure 5. Interaction of MBNL truncations with PTB. (**A**) Schematic representation of Venus-tagged MBNL1 fusion proteins with the amino acid boundaries indicated (upper). Black boxes represent the four ZF domains, the grey shaded box the C-terminus and the yellow dot the Venus tag. Schematic representation of mCherry-tagged PTB (lower); white numbered boxes represent the RRM domains and 'L' denotes inter-RRM linkers. (**B**) Western blot of input (left panel, 10% of immunoprecipitation) and anti-flag immunoprecipitation (right panel) of Venus–MBNL1 co-expressed with FLAG–PTB4 in formaldehyde cross-linked 293 T extracts. All lanes had FLAG–PTB4 co-expressed with Venus-tagged proteins; vector (lanes 1 and 10), MBNL1-2–382 (lanes 2 and 11), MBNL1-2–253 (lanes 3 and 12), MBNL1-2–183 (lanes 4 and 13), MBNL1-2–115 (lanes 5 and 14),

(continued)

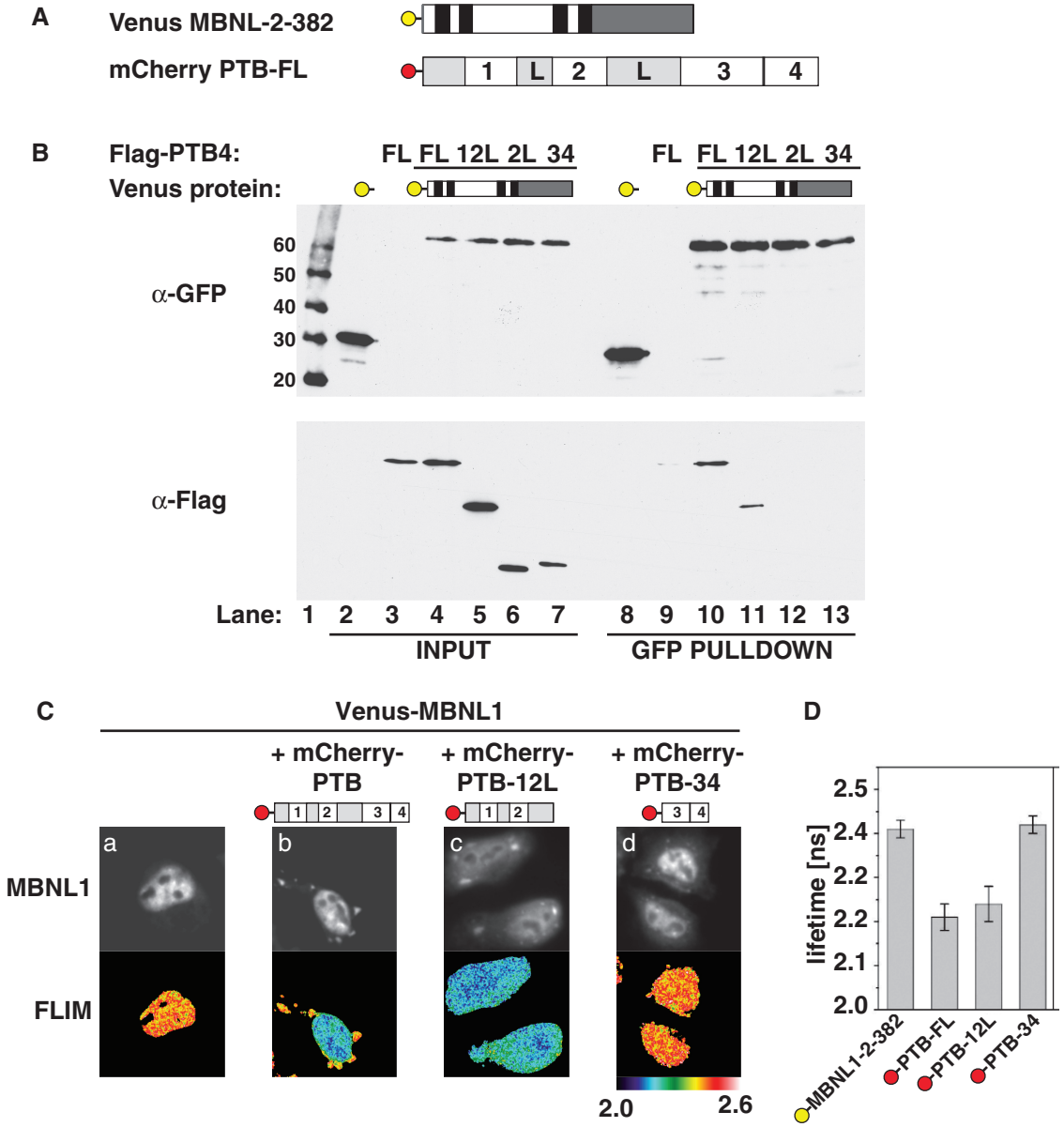

Figure 6. Interaction between MBNL and PTB N-terminal domains. (**A**) Schematic representation of Venus–MBNL and Cherry–PTB proteins. (**B**) Western blot of input (left panel) and GFP Trap (right panel) of Venus-tagged MBNL1 co-expressed with FLAG–PTB4 RRM domains in formaldehyde cross-linked 293 T extracts; markers (lane 1), Venus vector alone (lane 2 and 8), full-length FLAG–PTB4 (lanes 3 and 9). Lanes 4–7 and 10–13 all have full-length Venus–MBNL1 together with full-length PTB4 (lanes 4 and 10), FLAG–PTB4-12 L (lanes 5 and 11), FLAG–PTB4-2 L (lanes 6 and 12) and FLAG–PTB4-34 (lanes 7 and 13). (**C**) For each panel the top image shows the Venus–MBNL1 fluorescence, and the lower image shows the corresponding fluorescence lifetime in absence (a) or presence of the indicated PTB constructs (b–d). Full-length PTB and the first 2 RRMs plus the following linker bind to MBNL1, as indicated by reduced fluorescence lifetime (b,c) On the other hand the C-terminus of PTB containing RRMs 3 and 4 (d) cannot bind to MBNL1 and no energy transfer occurred with Cherry fused to either terminus of PTB-34. Scale bar = 10 μm. (**D**) Schematic presentation of tagged PTB RRMs and the statistical analysis of (B). Error bars are SEM of at least five independent fields of view with approximately four cells per image.

Figure 5. Continued
MBNL1-2–88 (lanes 6 and 15), MBNL1-2–104 (lanes 7 and 16), MBNL1-2–72 (lanes 8 and 17) and MBNL1-239–382 (lanes 9 and 18). Top panel, anti-PTB western, lower panel, anti-GFP western. (**C**) FLIM–FRET analysis of MBNL1 interaction with PTB. MBNL1 and PTB were fused to Venus as the FRET donor or mCherry as the acceptor and expressed in HeLa cells as indicated. MBNL fusion constructs are indicated with the N-terminal ZFs shown in black, and the C-terminal region shaded. First two rows show the Venus fluorescence and the corresponding fluorescence lifetime images of the indicated MBNL1 constructs in absence or presence of full-length mCherry–PTB, respectively. Third row shows the corresponding histograms (red line = donor only control; blue line = double transfection FRET). An energy transfer and, therefore, a reduction of the fluorescence lifetime was observed for N- (a) and C-terminal (b) labelled full-length MBNL1 (Venus–MBNL-2–382 and MBNL-2–382–Venus, respectively) in presence of mCherry-tagged PTB. Furthermore, the N-terminus of MBNL1 was sufficient to establish this interaction (c), whereas the C-terminal end alone did not show a FRET (d). (**D**) Statistical analysis of (C). Error bars are SEM of at least five independent fields of view with approximately four cells per image. Scale bar = 10 μm.

fusion proteins containing MBNL1 amino acids 2–116, 2–91 and 2–72, and also a 2–116-m protein with point mutations that impair RNA binding by ZnF1 and 2 and also abolish its activity in an MS2 tethering assay (C. Edge *et al*. in preparation). These fragments were chosen on the basis that 2–116 maintained high levels of activity in HeLa cells when tethered at the U or D position, whereas 2–72 had little residual activity (Figure 4). The GST–MBNL fusion proteins were bound to glutathione sepharose beads and then incubated in HeLa cell nuclear extract in the presence or absence of RNases. Beads were washed, and bound proteins were eluted in SDS loading buffer. A prominent 57/59 kDa doublet was pulled down by 2–116 in the absence of RNase, but not with the 2–72 construct or after treatment with RNase (Figure 7A). The 57/59 kDa doublet is the characteristic size of PTB, and its identity was confirmed by mass spectrometry (data not shown). Western blotting further confirmed that PTB was pulled down by 2–116 in the absence of RNase, but not by the 2–116-m RNA-binding mutant or the 2–72 proteins (Figure 7B). RNase sensitive interactions between RNA-binding proteins might be explained by independent binding of each protein to a common 'bridging' RNA, and they are often dismissed as non-specific. Nevertheless, the RNA-dependent interaction between PTB and MBNL1 2–116 showed some specificity because other abundant hnRNP proteins (hnRNPs C, H, L) were not pulled down (Figure 7B).

The preceding data suggested that RNAs present in HeLa nuclear extract mediate the observed interaction between MBNL1 and PTB. The simplest explanation is the presence in the extract of bridging RNAs containing binding sites for both proteins. Consistent with this, supplementation of *Tpm1* RNA 'a', which contains PTB- and MBNL1-binding elements (Figure 7C), led to a large increase in the quantity of HeLa PTB pulled down with MBNL1 2–116 (Figure 7D, lanes 2–5). However, titration of an MBNL1 SELEX winner sequence (40) also increased the amount of PTB pulled down (Figure 7D, lanes 6–8), even though this RNA does not bind to PTB (Figure 7E, lane 1). In contrast, a PTB SELEX RNA, which binds PTB but not MBNL (Figure 7E, lanes 3 and 4) did not increase PTB pull-down (Figure 7D, lanes 9–11). Enhanced pull-down of PTB by the MBNL1 SELEX RNA was not inhibited by the addition of PTB SELEX RNA (Figure 7D, lanes 12–14). This observation strongly argues that the RNA-dependent interaction does not require bridging RNAs. These data suggest that the interaction of PTB with MBNL1 2–116 is promoted by binding of MBNL1 to RNA via its ZnF1 and 2 domains, possibly via an RNA-binding–induced conformational change in MBNL1.

We next asked whether we could observe interaction between purified recombinant GST–MBNL1 and His_6–PTB proteins (Figure 7F and G). Pull-down was carried out using glutathione beads and analysed by SDS–PAGE. His_6–PTB was not pulled down by GST alone (Figure 7F, lane 3). GST–MBNL1 2–253 pulled down detectable amounts of His_6–PTB in the absence of added RNA (Figure 7F, lanes 6, 10, 14 and 18). Titration of Tpm1 RNA 'a' led to increased His_6–PTB pull-down (lanes 7–9), consistent with the presence of binding sites for both PTB and MBNL in this RNA (Figure 3). However, as in the nuclear extract experiments, the MBNL1 SELEX RNA (Figure 7F, lanes 11–13), but not the PTB SELEX RNA (lanes 15–17), induced pull-down of His_6–PTB. The *Tpm1* D element (RNA 'f'), which binds MBNL but not PTB (Figure 3C, lane 9), also induced His_6–PTB pull-down (lanes 19–21). These data support a model in which RNA binding by MBNL1 promotes its interaction with PTB.

Finally, we compared different MBNL deletion proteins in the reconstituted pull-down assay in the presence or absence of the D element containing RNA 'f' (Figure 7G). The 2–253, 2–116 and 2–91 MBNL1 proteins all showed enhanced (2.2- to 2.5-fold) PTB pull-down in response to the D-element RNA (Figure 7G, lanes 1–4, 7 and 8). In contrast, the 2–72 and 2–116 m with RNA-binding mutations showed lower levels of pull-down that were unresponsive to RNA (lanes 5, 6, 9 and 10).

DISCUSSION

Our findings demonstrate that MBNL promotes skipping of *Tpm1* exon 3 in close collaboration with PTB. This contrasts with the majority of events regulated by MBNL, where there is little evidence to suggest that the two proteins act in concert. Both PTB and MBNL proteins regulate striated muscle-specific splicing events [reviewed in (8)], and a computationally assembled splicing code showed significant co-association of MBNL and PTB motifs with striated muscle-specific exons (48). Based on the known expression and position-dependent activity of PTB and MBNL (34,38–40,49), it seems that PTB and MBNL act independently and with opposing activities to promote striated muscle-specific exon inclusion: PTB as a repressor in non-muscle cells, and MBNL as an activator in muscle cells. Exon 5 of cardiac troponin T is regulated negatively by both PTB and MBNL (30,34,50). However, in this case, PTB acts by antagonizing the binding of activator CELF proteins at muscle-specific enhancer elements (50), while later in development MBNL binds to sites that directly compete with U2AF65 binding (51). In contrast, we show that MBNL and PTB act together, via a direct physical interaction, to repress splicing of *Tpm1* exon 3.

The interaction between PTB and MBNL, promoted by RNA binding to MBNL, is perhaps our most intriguing finding. RNA-dependent protein-to-protein interactions are often dismissed as non-specific interactions mediated by RNAs bearing binding sites for the two proteins of interest. Several observations argue against this potentially trivial explanation for the PTB–MBNL interaction. First, GST–MBNL1 2–116 pulled down PTB but not several other abundant hnRNPs from HeLa extracts (Figure 7), including hnRNP H, which has been reported to interact with MBNL (52). By itself, this observation does not argue directly against RNA-bridged interactions, although it would indicate that any such interactions are highly selective for association of MBNL with PTB on the same RNAs. Second, the

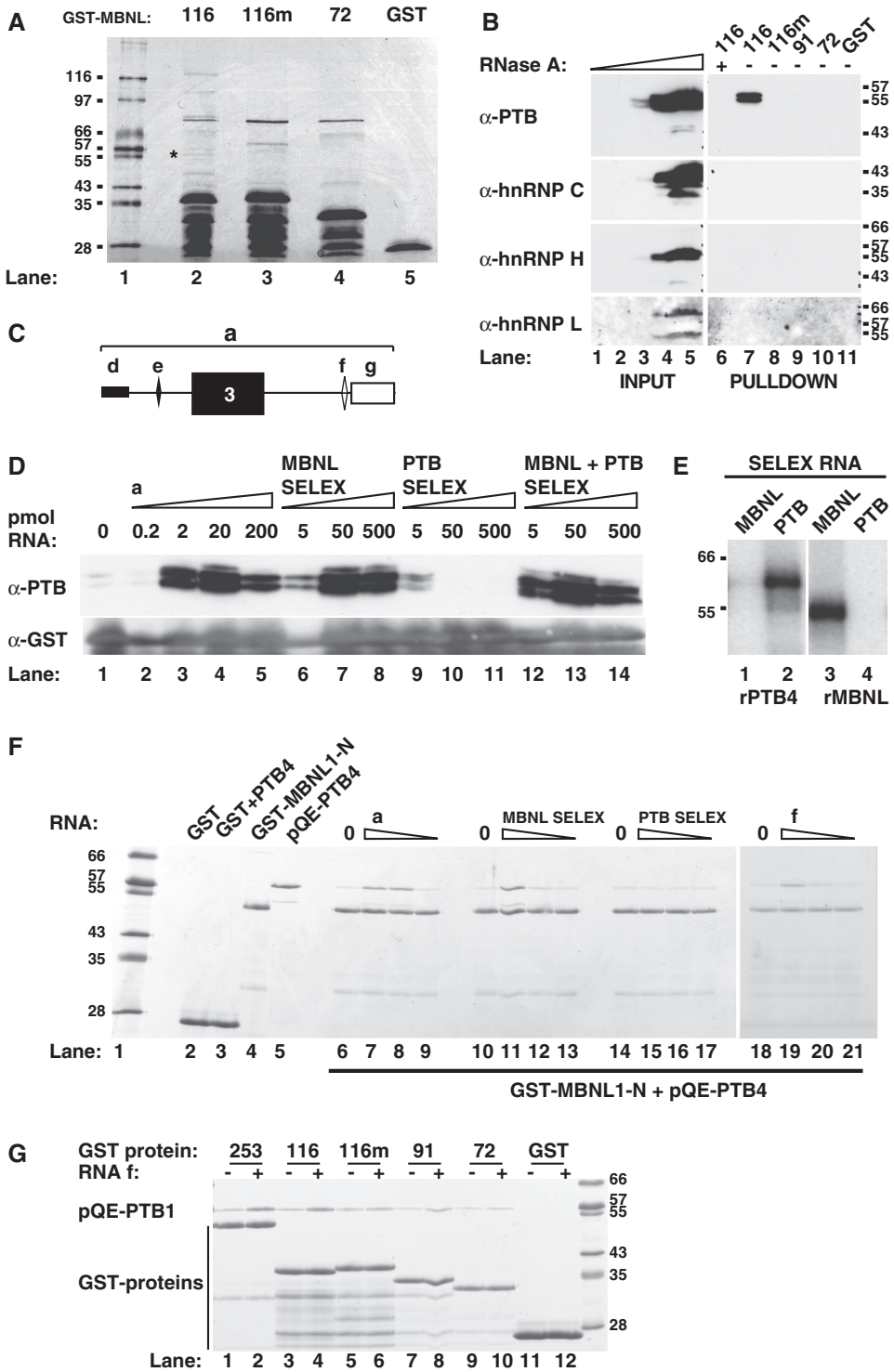

Figure 7. RNA binding by MBNL1 enhances the interaction with PTB. (**A**) Silver stain gel of GST pull-down in HeLa nuclear extract with GST-MBNL-2–116, 2–116 m, 2–72 and GST alone (lanes 2–6). The doublet identified by mass spectrometry as PTB is marked by an asterisk. This doublet was not observed if extract was treated with RNase. (**B**) Western blot of pull-down from A probing with anti-PTB, anti-hnRNP C, anti-hnRNP H and anti-hnRNP L (right panel) with a titration of the input 0.01, 0.1, 1, 10 and 100% (left panel). (**C**) Schematic diagram of *Tpm1* RNA species used in panels D, F and G. (**D**) Western blots using anti-PTB (upper panel) and anti-GST (lower panel). GST–MBNL-2–116 pull-down in HeLa nuclear extract with increasing amounts of RNA. No RNA added (lane 1), RNA a (lanes 2–5, Figure 3), MBNL SELEX RNA (lanes 6–8), PTB SELEX RNA (lanes 9–11), MBNL and PTB SELEX RNAs together (lanes 12–14). (**E**) UV X-linking of recombinant pQE–PTB4, left panel, or GST–MBNL1 amino acids 2–253, right panel, to either the MBNL SELEX RNA, lanes 1 and 3, or the PTB SELEX RNA, lanes 2 and 4. (**F**) GST pull-down with recombinant GST–MBNL1 amino acids 2–253 and pQE–PTB4 with a titration of RNA. Markers (lane 1), recombinant GST protein bound to beads minus and plus recombinant pQE–PTB4 (lanes 2 and 3), recombinant GST–MBNL1-2–253 bound to beads (lane 4, input), recombinant pQE–PTB4 (lane 5, 15% of input), GST–MBNL beads plus pQE–PTB4 (lanes 6–21) with no RNA added (lanes 6, 10, 14 and 18), titration of RNA a (20, 2 and 0.2 pmol, lanes 7–9), titration of MBNL SELEX (20, 2 and 0.2 pmol, lanes 11–13), titration of PTB SELEX (20, 2 and 0.2 pmol, lanes 15–17) and titration of RNA f (20, 2 and 0.2 pmol, lanes 19–21). (**G**) GST pull-down with recombinant GST–MBNL1 C-terminal truncations indicated and pQE–PTB4 minus RNA (lanes 1, 3, 5, 7, 9 and 11) and plus 40 pmol RNA f (lanes 2, 4, 6, 8, 10 and 12).

interaction in nuclear extracts, or with purified proteins, was promoted by RNAs that can bind MBNL but not PTB (Figure 7D–G). Third, PTB SELEX RNA did not inhibit the MBNL SELEX stimulated interaction, as would be predicted for a bridged interaction (Figure 7D). Taken together, these observations suggest an alternative to an RNA-bridged interaction, namely, that RNA binding by MBNL1 ZF1 and 2 induces a conformational change that favours interaction with PTB. Although RNA binding is well known to induce conformational changes in enzymes, such as RNA helicases and ATPases, RNA binding by domains, such as RRM, KH and ZF domains, has not generally been associated with large-scale conformational changes. Indeed, the published structures of MBNL1 ZF domains in free and RNA-bound form do not give direct insights into the nature of the conformational change suggested by our data. The structures of RNA-bound and free forms of MBNL1 ZF3 and 4 are almost identical (C_α r.m.s. deviation of 1.1 Å), but the structure of the ZF1 and 2 di-domain has only been solved in the free form (36). Compared with the other domains, ZF2 of MBNL1 and 2 contains an extended C-terminal α helix (35,36), but the crystallized fragment only extends to amino acid 90, whereas efficient interaction with PTB required amino acids up to 116 (Figure 7). It is possible that an ordered structure encompassing MBNL1 residues 90–116 only occurs in a ternary complex of MBNL1 with RNA and PTB, or potentially other interacting proteins.

Although the specificity of the MBNL–PTB interaction is supported by the preceding lines of evidence, the fact that it could not be detected by conventional co-immunoprecipitation or in a native electrophoretic mobility shift assay (data not shown) suggests that the interaction may not be stable under some experimental conditions. Likewise, the minimal region of MBNL required for interaction with PTB varied according to the experimental method. Amino acids 2–72, encompassing the core of ZF1 and 2, but lacking the C-terminal α-helical extension seen in the crystal structure (36), was seen to interact by co-immunoprecipitation after formaldehyde cross-linking (Figure 5), but not in the nuclear extract assays (Figure 7A and B) and only weakly with purified components (Figure 7F and G). The formaldehyde treatment might stabilize weak non-functional interactions that cannot be observed by other methods. The correlation between fragments of MBNL that were active in the tethered function assay and that were able to interact with PTB was imperfect, in part because of the variable response in different tethering (Figure 4) and PTB interaction assays (Figures 5–7). Nevertheless, most of the active tethered fragments also interacted with PTB in at least one assay. Moreover, the mutations of MBNL1 2–116 that impair the ability to interact with PTB also neutralize its activity in a tethered function assay (C. Edge *et al*. in preparation). This loss of activity could be related to both binding to a specific *cis* RNA element, as well as the activated interaction with PTB. In simple co-transfection assays, all tested deletions of MBNL1 lost activity on our *Tpm1* reporter (Figure 1). In contrast, the Cooper laboratory was able to identify by deletion separate regions of MBNL1 and 3 required for splicing repression or activation in similar co-transfection assays (53). Repression of cTnT exon 5 required a region encompassing MBNL1 ZnF1 and 2, as well as an additional 80 amino acids. This is similar to the minimal repressor region of MBNL1 that we identified via the MS2 tethering assay (Figure 4). Whether MBNL repression of cTnT is related to PTB, or some other interacting protein, is an open question.

MBNL proteins can activate or repress target exons (29–33,38–40,51). In common with other RNA-binding proteins (6), MBNL1 tends to repress when bound upstream and activate when bound downstream of a target cassette exon (38–40). *Tpm1* exon 3 is distinct from other MBNL-regulated events both in the concerted action of MBNL1 and PTB to confer a smooth muscle splicing pattern, and in the wide separation of MBNL1-binding sites flanking the target exon. The location of upstream MBNL sites in genes, such as *cTnT*, *Tnnt3* and *CLCN1*, is consistent with binding competition with splicing factors, such as U2AF65 (31–33,51). By contrast, neither the U nor D elements of *Tpm1* overlap constitutive splicing elements, as illustrated by the lack of impairment of splicing when they are replaced by MS2 sites (Figure 4). The D element is ∼140 nt downstream of the exon, whereas the U element is 60 nt upstream of the 3′ splice site, and at least 40 nt downstream of the polypyrimidine tract (14,16). Therefore, repression of *Tpm1* exon 3 is unlikely to involve direct binding competition of MBNL1 with splicing factors as in *cTnT* (32,51).

Each of the two MBNL1-binding sites lies close to a PTB-binding polypyrimidine tract, which is more distant from the exon than the MBNL1 sites (17,18). Single molecule analysis of GFP–PTB in nuclear extracts shows that the P3 tract binds 3 PTB molecules, whereas DY binds two (20). Although the downstream PTB-binding sites are also remote from any constitutive splice elements, the upstream sites are embedded within the P3 pyrimidine tract, which binds U2AF65 and is associated with the branch point (17). A plausible way in which MBNL1 proteins might contribute to repression of *Tpm1* exon 3 is via stabilization of PTB binding so that it is resistant to displacement by splicing factors, such as U2AF. The observed interaction between PTB and MBNL (Figures 5–7) and the positive effect of the MBNL-binding sites on the occupancy of PTB sites on *Tpm1* RNA supports such a model. However, regulation of *Tpm1* splicing requires all elements flanking exon 3; therefore, it cannot be explained simply by cooperative binding of PTB and MBNL to adjacent binding sites.

Co-immunoprecipitation and yeast two-hybrid analysis indicate that MBNL1 monomers interact via the C-terminal region (33,54), which may account for the residual activity of the C-terminal region in MS2 tethering assays (Figure 4). This suggests a model for regulation of *Tpm1* splicing in which MBNL proteins bound to the U and D elements interact directly with each other, thereby looping out exon 3 (20). In principle, the single molecule TIRF experiments could provide useful insights by revealing the stoichiometry of MBNL binding to the *Tpm1* RNAs. In practice, although the TIRF analyses gave

reliable data on co-localization of MBNL with labelled RNA and suggested binding of multiple MBNL molecules to individual RNAs, it was not possible to model the data unambiguously. We suspect that this was due to the presence of multiple sites of different affinities together with low concentrations of MBNL1–GFP (~0.5 μM) in nuclear extracts. Nevertheless, it remains possible that bridging of the U and D elements by two or more MBNL molecules would bring the two PTB-binding tracts into closer proximity, an effect that would be further enhanced by the direct interaction between MBNL and PTB (Figures 5–7). The co-repressor Raver1 could also contribute to stabilization or formation of such a complex by binding to two or more PTB monomers (24). However, there is no direct evidence for such a looped complex, and it remains possible that the upstream and downstream repressive PTB–MBNL complexes act independently to repress exon 3.

A major issue that our experiments have not addressed is the nature of the switch between contractile smooth muscle cells, where PTB and MBNL act to repress *Tpm1* exon 3 and other cells where exon 3 is selected. Although PTB and MBNL are part of the essential repressive machinery in smooth muscle cells, their mRNA expression levels do not seem to alter substantially during de-differentiation of mouse aorta and bladder smooth muscle cells (M. Hallegger and C.W.J.S. unpublished observations). This contrasts with developing cardiac muscle where changes in levels of MBNL and CELF proteins correlate with alterations in target splicing events (30,34,50). Explanations for the switch in *Tpm1* splicing could include regulation of PTB or MBNL by post-translational modifications, or alterations in the activities of other positive or negatively acting factors. The fact that the MS2-tethering assays showed a greater sensitivity to deletions in PAC1 cells than in HeLa cells (Figure 4) hints that additional functional interactions, notably with the C-terminal region of MBNL1, might occur in smooth muscle cells. Furthermore, the branch point mutation in the pTΔBP reporter used in HeLa cells might bypass the need for some regulatory influences despite its continued dependence on all regulatory elements (Supplementary Figure S1). Finally, multiple MBNL proteins arise via alternative splicing from the MBNL1, 2 and 3 genes (55). Here, we have focused on one particular isoform of MBNL1. However, MBNL isoforms differ in various functional properties (54); therefore, it is an interesting possibility that other MBNL isoforms might be more active for repression of *Tpm1* exon 3. Future work will also need to address the fact that although both the U and D elements bind MBNL (Figure 3), and their activity can be replaced by artificially tethered MBNL (Figure 4), they are not functionally interchangeable (16), which could be related to differential binding of MBNL isoforms.

SUPPLEMENTARY DATA

Supplementary Data are available at NAR Online: Supplementary Figures 1–4.

ACKNOWLEDGEMENTS

The authors thank T. Cooper for the GFP MBNL41 plasmid, J. Caceres for the pCGTHCF$_{FL}$T7 vector used for the expression of MBNL1 in 293T cells, P. Whitfield for help in developing the MS2 recruitment of MBNL to the sites upstream of *Tpm1* exon 3, D. Black and J. Ule for antibodies and B. Luisi for helpful comments on the manuscript.

FUNDING

Wellcome Trust programme [092900 to C.W.J.S.]; Max-Planck Society (to M.L.); Biotechnology and Biological Sciences Research Council studentship (to C.E.); Wellcome Trust Value In People award [088113/Z/08/Z to D.C.]; Wellcome Trust [089703/Z/09/Z to C.F.K.]; Medical Research Council [MR/K015850/1 to C.F.K.]; Alzheimer Research UK Trust [ARUK-EG2012A-1 to C.F.K.]; Engineering and Physical Sciences Research Council [EP/H018301/1 to C.F.K.]. Funding for open access charge: Wellcome Trust grant.

Conflict of interest statement. None declared.

REFERENCES

1. Wang,E.T., Sandberg,R., Luo,S., Khrebtukova,I., Zhang,L., Mayr,C., Kingsmore,S.F., Schroth,G.P. and Burge,C.B. (2008) Alternative isoform regulation in human tissue transcriptomes. *Nature*, **456**, 470–476.
2. Pan,Q., Shai,O., Lee,L.J., Frey,B.J. and Blencowe,B.J. (2008) Deep surveying of alternative splicing complexity in the human transcriptome by high-throughput sequencing. *Nat. Genet.*, **40**, 1413–1415.
3. Nilsen,T.W. and Graveley,B.R. (2010) Expansion of the eukaryotic proteome by alternative splicing. *Nature*, **463**, 457–463.
4. Chen,M. and Manley,J.L. (2009) Mechanisms of alternative splicing regulation: insights from molecular and genomics approaches. *Nat. Rev. Mol. Cell Biol.*, **10**, 741–754.
5. Matlin,A.J., Clark,F. and Smith,C.W. (2005) Understanding alternative splicing: towards a cellular code. *Nat. Rev. Mol. Cell Biol.*, **6**, 386–398.
6. Witten,J.T. and Ule,J. (2011) Understanding splicing regulation through RNA splicing maps. *Trends Genet.*, **27**, 89–97.
7. Li,Q., Lee,J.A. and Black,D.L. (2007) Neuronal regulation of alternative pre-mRNA splicing. *Nat. Rev. Neurosci.*, **8**, 819–831.
8. Llorian,M. and Smith,C.W. (2011) Decoding muscle alternative splicing. *Curr. Opin. Genet. Dev.*, **21**, 380–387.
9. Gooding,C. and Smith,C.W. (2008) Tropomyosin exons as models for alternative splicing. *Adv. Exp. Med. Biol.*, **644**, 27–42.
10. Wieczorek,D.F., Smith,C.W. and Nadal-Ginard,B. (1988) The rat alpha-tropomyosin gene generates a minimum of six different mRNAs coding for striated, smooth, and nonmuscle isoforms by alternative splicing. *Mol. Cell Biol.*, **8**, 679–694.
11. Ellis,P.D., Smith,C.W. and Kemp,P. (2004) Regulated tissue-specific alternative splicing of enhanced green fluorescent protein transgenes conferred by alpha-tropomyosin regulatory elements in transgenic mice. *J. Biol. Chem.*, **279**, 36660–36669.
12. Mullen,M.P., Smith,C.W., Patton,J.G. and Nadal-Ginard,B. (1991) Alpha-tropomyosin mutually exclusive exon selection: competition between branchpoint/polypyrimidine tracts determines default exon choice. *Genes Dev.*, **5**, 642–655.
13. Rothman,A., Kulik,T.J., Taubman,M.B., Berk,B.C., Smith,C.W. and Nadal-Ginard,B. (1992) Development and characterization of a cloned rat pulmonary arterial smooth muscle cell line that maintains differentiated properties through multiple subcultures. *Circulation*, **86**, 1977–1986.

14. Gooding,C., Roberts,G.C., Moreau,G., Nadal-Ginard,B. and Smith,C.W. (1994) Smooth muscle-specific switching of alpha-tropomyosin mutually exclusive exon selection by specific inhibition of the strong default exon. *EMBO J.*, **13**, 3861–3872.
15. Smith,C.W. and Nadal-Ginard,B. (1989) Mutually exclusive splicing of alpha-tropomyosin exons enforced by an unusual lariat branch point location: implications for constitutive splicing. *Cell*, **56**, 749–758.
16. Gromak,N. and Smith,C.W. (2002) A splicing silencer that regulates smooth muscle specific alternative splicing is active in multiple cell types. *Nucleic Acids Res.*, **30**, 3548–3557.
17. Perez,I., Lin,C.H., McAfee,J.G. and Patton,J.G. (1997) Mutation of PTB binding sites causes misregulation of alternative 3′ splice site selection in vivo. *RNA*, **3**, 764–778.
18. Gooding,C., Roberts,G.C. and Smith,C.W. (1998) Role of an inhibitory pyrimidine element and polypyrimidine tract binding protein in repression of a regulated alpha-tropomyosin exon. *RNA*, **4**, 85–100.
19. Wollerton,M.C., Gooding,C., Robinson,F., Brown,E.C., Jackson,R.J. and Smith,C.W. (2001) Differential alternative splicing activity of isoforms of polypyrimidine tract binding protein (PTB). *RNA*, **7**, 819–832.
20. Cherny,D., Gooding,C., Eperon,G.E., Coelho,M.B., Bagshaw,C.R., Smith,C.W. and Eperon,I.C. (2010) Stoichiometry of a regulatory splicing complex revealed by single-molecule analyses. *EMBO J.*, **29**, 2161–2172.
21. Roberts,G.C., Gooding,C. and Smith,C.W. (1996) Smooth muscle alternative splicing induced in fibroblasts by heterologous expression of a regulatory gene. *EMBO J.*, **15**, 6301–6310.
22. Huttelmaier,S., Illenberger,S., Grosheva,I., Rudiger,M., Singer,R.H. and Jockusch,B.M. (2001) Raver1, a dual compartment protein, is a ligand for PTB/hnRNPI and microfilament attachment proteins. *J. Cell Biol.*, **155**, 775–786.
23. Gromak,N., Rideau,A., Southby,J., Scadden,A.D., Gooding,C., Huttelmaier,S., Singer,R.H. and Smith,C.W. (2003) The PTB interacting protein raver1 regulates alpha-tropomyosin alternative splicing. *EMBO J.*, **22**, 6356–6364.
24. Rideau,A.P., Gooding,C., Simpson,P.J., Monie,T.P., Lorenz,M., Huttelmaier,S., Singer,R.H., Matthews,S., Curry,S. and Smith,C.W. (2006) A peptide motif in Raver1 mediates splicing repression by interaction with the PTB RRM2 domain. *Nat. Struct. Mol. Biol.*, **13**, 839–848.
25. Joshi,A., Coelho,M.B., Kotik-Kogan,O., Simpson,P.J., Matthews,S.J., Smith,C.W.J. and Curry,S. (2011) Crystallographic analysis of polypyrimidine tract-binding protein-Raver1 interactions involved in regulation of alternative splicing. *Structure*, **19**, 1816–1825.
26. Lee,J.H., Rangarajan,E.S., Yogesha,S.D. and Izard,T. (2009) Raver1 interactions with vinculin and RNA suggest a feed-forward pathway in directing mRNA to focal adhesions. *Structure*, **17**, 833–842.
27. Lahmann,I., Fabienke,M., Henneberg,B., Pabst,O., Vauti,F., Minge,D., Illenberger,S., Jockusch,B.M., Korte,M. and Arnold,H.H. (2008) The hnRNP and cytoskeletal protein raver1 contributes to synaptic plasticity. *Exp. Cell Res.*, **314**, 1048–1060.
28. Ladd,A.N., Charlet,N. and Cooper,T.A. (2001) The CELF family of RNA binding proteins is implicated in cell-specific and developmentally regulated alternative splicing. *Mol. Cell Biol.*, **21**, 1285–1296.
29. Hino,S., Kondo,S., Sekiya,H., Saito,A., Kanemoto,S., Murakami,T., Chihara,K., Aoki,Y., Nakamori,M., Takahashi,M.P. *et al.* (2007) Molecular mechanisms responsible for aberrant splicing of SERCA1 in myotonic dystrophy type 1. *Hum. Mol. Genet.*, **16**, 2834–2843.
30. Ho,T.H., Charlet,B.N., Poulos,M.G., Singh,G., Swanson,M.S. and Cooper,T.A. (2004) Muscleblind proteins regulate alternative splicing. *EMBO J.*, **23**, 3103–3112.
31. Kino,Y., Washizu,C., Oma,Y., Onishi,H., Nezu,Y., Sasagawa,N., Nukina,N. and Ishiura,S. (2009) MBNL and CELF proteins regulate alternative splicing of the skeletal muscle chloride channel CLCN1. *Nucleic Acids Res.*, **37**, 6477–6490.
32. Warf,M.B. and Berglund,J.A. (2007) MBNL binds similar RNA structures in the CUG repeats of myotonic dystrophy and its pre-mRNA substrate cardiac troponin T. *RNA*, **13**, 2238–2251.
33. Yuan,Y., Compton,S.A., Sobczak,K., Stenberg,M.G., Thornton,C.A., Griffith,J.D. and Swanson,M.S. (2007) Muscleblind-like 1 interacts with RNA hairpins in splicing target and pathogenic RNAs. *Nucleic Acids Res.*, **35**, 5474–5486.
34. Kalsotra,A., Xiao,X., Ward,A.J., Castle,J.C., Johnson,J.M., Burge,C.B. and Cooper,T.A. (2008) A postnatal switch of CELF and MBNL proteins reprograms alternative splicing in the developing heart. *Proc. Natl Acad. Sci. USA*, **105**, 20333–20338.
35. He,F., Dang,W., Abe,C., Tsuda,K., Inoue,M., Watanabe,S., Kobayashi,N., Kigawa,T., Matsuda,T., Yabuki,T. *et al.* (2009) Solution structure of the RNA binding domain in the human muscleblind-like protein 2. *Protein Sci.*, **18**, 80–91.
36. Teplova,M. and Patel,D.J. (2008) Structural insights into RNA recognition by the alternative-splicing regulator muscleblind-like MBNL1. *Nat. Struct. Mol. Biol.*, **15**, 1343–1351.
37. Miller,J.W., Urbinati,C.R., Teng-Umnuay,P., Stenberg,M.G., Byrne,B.J., Thornton,C.A. and Swanson,M.S. (2000) Recruitment of human muscleblind proteins to (CUG)(n) expansions associated with myotonic dystrophy. *EMBO J.*, **19**, 4439–4448.
38. Du,H., Cline,M.S., Osborne,R.J., Tuttle,D.L., Clark,T.A., Donohue,J.P., Hall,M.P., Shiue,L., Swanson,M.S., Thornton,C.A. *et al.* (2010) Aberrant alternative splicing and extracellular matrix gene expression in mouse models of myotonic dystrophy. *Nat. Struct. Mol. Biol.*, **17**, 187–193.
39. Wang,E.T., Cody,N.A., Jog,S., Biancolella,M., Wang,T.T., Treacy,D.J., Luo,S., Schroth,G.P., Housman,D.E., Reddy,S. *et al.* (2012) Transcriptome-wide regulation of pre-mRNA splicing and mRNA localization by muscleblind proteins. *Cell*, **150**, 710–724.
40. Goers,E.S., Purcell,J., Voelker,R.B., Gates,D.P. and Berglund,J.A. (2010) MBNL1 binds GC motifs embedded in pyrimidines to regulate alternative splicing. *Nucleic Acids Res.*, **38**, 2467–2484.
41. Cass,D., Hotchko,R., Barber,P., Jones,K., Gates,D.P. and Berglund,J.A. (2011) The four Zn fingers of MBNL1 provide a flexible platform for recognition of its RNA binding elements. *BMC Mol. Biol.*, **12**, 20.
42. Gooding,C., Clark,F., Wollerton,M.C., Grellscheid,S.N., Groom,H. and Smith,C.W. (2006) A class of human exons with predicted distant branch points revealed by analysis of AG dinucleotide exclusion zones. *Genome Biol.*, **7**, R1.
43. Cazalla,D., Sanford,J.R. and Caceres,J.F. (2005) A rapid and efficient protocol to purify biologically active recombinant proteins from mammalian cells. *Protein Expr. Purif.*, **42**, 54–58.
44. Del Gatto-Konczak,F., Olive,M., Gesnel,M.C. and Breathnach,R. (1999) hnRNP A1 recruited to an exon in vivo can function as an exon splicing silencer. *Mol. Cell Biol.*, **19**, 251–260.
45. Robinson,F. and Smith,C.W. (2006) A splicing repressor domain in polypyrimidine tract-binding protein. *J. Biol. Chem.*, **281**, 800–806.
46. Dignam,J.D., Lebovitz,R.M. and Roeder,R.G. (1983) Accurate transcription initiation by RNA polymerase II in a soluble extract from isolated mammalian nuclei. *Nucleic Acids Res.*, **11**, 1475–1489.
47. Lorenz,M. (2009) Visualizing protein-RNA interactions inside cells by fluorescence resonance energy transfer. *RNA*, **15**, 97–103.
48. Barash,Y., Calarco,J.A., Gao,W., Pan,Q., Wang,X., Shai,O., Blencowe,B.J. and Frey,B.J. (2010) Deciphering the splicing code. *Nature*, **465**, 53–59.
49. Llorian,M., Schwartz,S., Clark,T.A., Hollander,D., Tan,L.Y., Spellman,R., Gordon,A., Schweitzer,A.C., de la Grange,P., Ast,G. *et al.* (2010) Position-dependent alternative splicing activity revealed by global profiling of alternative splicing events regulated by PTB. *Nat. Struct. Mol. Biol.*, **17**, 1114–1123.
50. Charlet,B.N., Logan,P., Singh,G. and Cooper,T.A. (2002) Dynamic antagonism between ETR-3 and PTB regulates cell type-specific alternative splicing. *Mol. Cell*, **9**, 649–658.
51. Warf,M.B., Diegel,J.V., von Hippel,P.H. and Berglund,J.A. (2009) The protein factors MBNL1 and U2AF65 bind alternative RNA structures to regulate splicing. *Proc. Natl Acad. Sci. USA*, **106**, 9203–9208.
52. Paul,S., Dansithong,W., Kim,D., Rossi,J., Webster,N.J., Comai,L. and Reddy,S. (2006) Interaction of muscleblind, CUG-BP1 and hnRNP H proteins in DM1-associated aberrant IR splicing. *EMBO J.*, **25**, 4271–4283.

53. Grammatikakis,I., Goo,Y.H., Echeverria,G.V. and Cooper,T.A. (2011) Identification of MBNL1 and MBNL3 domains required for splicing activation and repression. *Nucleic Acids Res.*, **39**, 2769–2780.
54. Tran,H., Gourrier,N., Lemercier-Neuillet,C., Dhaenens,C.M., Vautrin,A., Fernandez-Gomez,F.J., Arandel,L., Carpentier,C., Obriot,H., Eddarkaoui,S. *et al.* (2011) Analysis of exonic regions involved in nuclear localization, splicing activity, and dimerization of muscleblind-like-1 isoforms. *J. Biol. Chem.*, **286**, 16435–16446.
55. Pascual,M., Vicente,M., Monferrer,L. and Artero,R. (2006) The muscleblind family of proteins: an emerging class of regulators of developmentally programmed alternative splicing. *Differentiation*, **74**, 65–80.